

# Combinatorial Effects of Alpha- and Gamma-Protocadherins on Neuronal Survival and Dendritic Self-Avoidance

Samantha Ing-Esteves,<sup>1</sup>  Dimitar Kostadinov,<sup>2</sup> Julie Marocha,<sup>1</sup>  Anson D. Sing,<sup>1</sup>  Kezia S. Joseph,<sup>1</sup> Mallory A. Laboulaye,<sup>2</sup>  Joshua R. Sanes,<sup>2\*</sup> and  Julie L. Lefebvre<sup>1,2\*</sup>

<sup>1</sup>Program for Neurosciences and Mental Health, Hospital for Sick Children, Department of Molecular Genetics, University of Toronto, Toronto, Ontario M5G 0A4, Canada and <sup>2</sup>Department of Molecular and Cellular Biology and Center for Brain Science, Harvard University, Cambridge, Massachusetts 02138

The clustered protocadherins (Pcdhs) comprise 58 cadherin-related proteins encoded by three tandemly arrayed gene clusters, *Pcdh- $\alpha$* , *Pcdh- $\beta$* , and *Pcdh- $\gamma$*  (*Pcdha*, *Pcdhb*, and *Pcdhg*, respectively). Pcdh isoforms from different clusters are combinatorially expressed in neurons. They form multimers that interact homophilically and mediate a variety of developmental processes, including neuronal survival, synaptic maintenance, axonal tiling, and dendritic self-avoidance. Most studies have analyzed clusters individually. Here, we assessed functional interactions between *Pcdha* and *Pcdhg* clusters. To circumvent neonatal lethality associated with deletion of *Pcdhgs*, we used Crispr-Cas9 genome editing in mice to combine a constitutive *Pcdha* mutant allele with a conditional *Pcdhg* allele. We analyzed roles of Pcdhas and Pcdhgs in the retina and cerebellum from mice (both sexes) lacking one or both clusters. In retina, Pcdhgs are essential for survival of inner retinal neurons and dendritic self-avoidance of starburst amacrine cells, whereas Pcdhas are dispensable for both processes. Deletion of both *Pcdha* and *Pcdhg* clusters led to far more dramatic defects in survival and self-avoidance than *Pcdhg* deletion alone. Comparisons of an allelic series of mutants support the conclusion that Pcdhas and Pcdhgs function together in a dose-dependent and cell-type-specific manner to provide a critical threshold of Pcdh activity. In the cerebellum, Pcdhas and Pcdhgs also cooperate to mediate self-avoidance of Purkinje cell dendrites, with modest but significant defects in either single mutant and dramatic defects in the double mutant. Together, our results demonstrate complex patterns of redundancy between Pcdh clusters and the importance of Pcdh cluster diversity in postnatal CNS development.

**Key words:** apoptosis; dendrite; neurite development; protocadherin; retina; self-avoidance

## Significance Statement

The formation of neural circuits requires diversification and combinatorial actions of cell surface proteins. Prominent among them are the clustered protocadherins (Pcdhs), a family of ~60 neuronal recognition molecules. Pcdhs are encoded by three closely linked gene clusters called *Pcdh- $\alpha$* , *Pcdh- $\beta$* , and *Pcdh- $\gamma$* . The Pcdhs mediate a variety of developmental processes, including neuronal survival, synaptic maintenance, and spatial patterning of axons and dendrites. Most studies to date have been limited to single clusters. Here, we used genome editing to assess interactions between *Pcdh- $\alpha$*  and *Pcdh- $\gamma$*  gene clusters. We examined two regions of the CNS, the retina and cerebellum and show that the 14  $\alpha$ -Pcdhs and 22  $\gamma$ -Pcdhs act synergistically to mediate neuronal survival and dendrite patterning.

## Introduction

The complexity of neural circuits in the CNS implies a corresponding complexity of molecular mechanisms to pattern pro-

jections and connections. An attractive hypothesis is that large families of recognition molecules underlie this specificity, with combinatorial expression of family members endowing neurons

Received Oct. 20, 2017; revised Jan. 12, 2018; accepted Jan. 29, 2018.

Author contributions: J.R.S. and J.L.L. designed research; S.I.-E., D.K., J.M., A.D.S., K.S.J., M.A.L., and J.L.L. performed research; S.I.-E., D.K., J.M., A.D.S., K.S.J., and J.L.L. analyzed data; J.R.S. and J.L.L. wrote the paper.

This work was supported by an Ontario Graduate Scholarship and a Vision Science Research Program Studentship from the University of Toronto (S.I.-E.); a University of Toronto Open Fellowship (J.M.); a Restrcomp Postdoctoral Fellowship from the Hospital for Sick Children (A.D.S.); a Canada Research Chair (Tier 2), a Sloan Fellowship in Neuroscience, an NSERC Discovery Grant (RPIN-2016-06128), the Hospital for Sick Children (J.L.L.); and the National Institutes of Health (Grants T32 EY007110 and F31 NS078893 to D.K. and Grant R01 EY022073 to J.R.S.). We thank Tom Maniatis and Weisheng Chen (Columbia University) for sharing the *Pcdha*<sup>ko</sup>, *Pcdhb*<sup>ko</sup>, and *Pcdha*<sup>tm<sup>cherry</sup></sup> mice

and tissue before publication and Tom Maniatis, Weisheng Chen, and members of the Lefebvre laboratory for helpful comments on this manuscript.

The authors declare no competing financial interests.

\*J.R.S. and J.L.L. are co-corresponding senior authors.

Correspondence should be addressed to Julie L. Lefebvre, Program for Neuroscience and Mental Health, Hospital for Sick Children, 686 Bay Street, Room 59707, Toronto M5G 0A4, Canada. E-mail: julie.lefebvre@sickkids.ca.

D. Kostadinov's present address: Wolfson Institute of Biomedical Research and Department of Neuroscience, Physiology and Pharmacology, University College London, London, UK.

DOI:10.1523/JNEUROSCI.3035-17.2018

Copyright © 2018 the authors 0270-6474/18/382713-17\$15.00/0

with distinct identities, patterning their axons and dendrites and biasing synapse formation in favor of appropriate partners (Zipursky and Sanes, 2010).

Candidate mediators of such processes include the clustered protocadherins (Pcdhs), a set of ~60 cadherin-related transmembrane molecules encoded by a tandem array of genes. *Pcdh* genes are subdivided into *Pcdh- $\alpha$*  (*Pcdha*), *Pcdh- $\beta$*  (*Pcdhb*), and *Pcdh- $\gamma$*  (*Pcdhg*) clusters, encoding 14, 22, and 22 isoforms, respectively, in mice (see Fig. 1A) (Wu and Maniatis, 1999). Most isoforms engage in strict homophilic binding in cell aggregation assays (Schreiner and Weiner, 2010; Thu et al., 2014). Isoforms from the same and different clusters form *cis*-dimers, which interact homophilically in *trans* in anti-parallel arrangements (Nicoludis et al., 2015; Rubinstein et al., 2015; Rubinstein et al., 2017). Pcdhs are expressed throughout the nervous system and expression is combinatorial and stochastic in at least some populations (Esumi et al., 2005; Kaneko et al., 2006; Toyoda et al., 2014; Mountoufaris et al., 2017). Therefore, Pcdhs are well suited to mediate complex, specific interactions among neurons.

Initial attempts to analyze Pcdh function used genetic methods to inactivate individual clusters. *Pcdhg* cluster mutations resulted in degenerative defects in the spinal cord and neonatal lethality (Wang et al., 2002). Subsequent studies using conditional *Pcdhg* mutants and hypomorphs documented neuronal death in several regions, as well as defects in synaptic maintenance and dendritic patterning (Weiner et al., 2005; Lefebvre et al., 2008; Prasad et al., 2008; Garrett and Weiner, 2009; Schreiner and Weiner, 2010; Su et al., 2010; Garrett et al., 2012; Lefebvre et al., 2012; Kostadinov and Sanes, 2015; Molumby et al., 2016). Inactivation of the *Pcdha* cluster resulted in abnormal axonal arborizations in several brain areas (Hasegawa et al., 2008; Katori et al., 2009; Meguro et al., 2015; Chen et al., 2017; Mountoufaris et al., 2017).

A second set of studies used loss- and gain-of-function strategies to assay roles of individual isoforms. Three noteworthy sets of results have been reported. The first distinguished two seemingly contradictory behaviors of retinal starburst amacrine cells (SACs). Dendrites of individual SACs repel each other in a process called self-avoidance, leading to even coverage of their receptive field. Simultaneously, however, SAC dendrites also synapse with dendrites of neighboring SACs, implying that they are capable of self-/non-self-discrimination. We showed that single *Pcdhg* isoforms can mediate self-avoidance, but multiple isoforms are required for self-/non-self-discrimination (Lefebvre et al., 2012; Kostadinov and Sanes, 2015). Second, whereas any *Pcdhg* isoform is sufficient for self-avoidance, neuronal survival in retina and spinal cord is dependent on the *PcdhgC3-C5* isoforms (Chen et al., 2012). Third, patterning of serotonergic axons is dependent on a single *Pcdha-C2* isoform (Chen et al., 2017).

A third level of complexity involves interactions among *Pcdh* gene clusters. Recently, two groups deleted the entire *Pcdh* locus in mice, revealing cooperation among clusters in patterning of olfactory axons and survival of spinal neurons (Hasegawa et al., 2016; Mountoufaris et al., 2017). In their alleles, the neonatal lethality of the *Pcdhg* mutation restricted analysis to embryos. In an independent approach, we have generated a mutant allele (*Pcdh-ag<sup>f</sup>*) in which constitutive *Pcdha* deletion is combined with conditional *Pcdhg* inactivation, circumventing neonatal lethality. Here, we compare phenotypes in single *Pcdha*, *Pcdhb*, and *Pcdhg* cluster mutants with those of *Pcdh-ag<sup>f</sup>* mutants, focusing on neuronal survival in retina and dendritic self-avoidance in retina and cerebellum. In retina, *Pcdhas* and *Pcdhbs* are dispensable on their own, but *Pcdh-ag* mutants dramatically enhance *Pcdhg* phenotypes, a phenomenon called unequal redundancy (Briggs et al.,

2006). In contrast, Purkinje cells are equally dependent on *Pcdha* and *Pcdhg* clusters for dendrite patterning, exhibiting partial redundancy. Together, the combined activities and diversity provided by the *Pcdh* clusters ensure robust neuronal patterning.

## Materials and Methods

**Mice.** To generate *Pcdh-ag<sup>f</sup>* mutants, a single guide RNA (sgRNA) targeting the *Pcdha* constant exon 1 was designed using a CRISPR design tool (<http://crispr.mit.edu/>). Oligo duplexes were annealed into pX330-U6-Chimeric\_BB-CBh-hSpCas9, a gift from Feng Zhang (Addgene, <https://www.addgene.org/search/advanced/?q=42230>; Cong et al., 2013). Multiple sgRNAs were screened in HEK293 cells for cleavage of target DNA sequence and disruption of *Pcdha*-exon1-GFP reporter expression. sgRNA for target 5'-CGCTAAGAGCAGGCATGCAC-3' was transcribed *in vitro* from pX330 with a T7 RNA polymerase (Ambion) and injected with Cas9 RNA (Systems Biosciences) into *Pcdh-g<sup>con3</sup>* zygotes at the Harvard University Genome Modification Facility (<https://gmf.fas.harvard.edu>, RRID:SCR\_009849). Of 220 zygotes injected, 16 pups were born and 11 pups had insertion or deletions in *Pcdha* constant exon 1 (*Pcdha<sup>conex1del</sup>*). Founders were identified by amplifying the targeted genomic region with primers, forward: 5' TTGGGCAGGGCACATCTAAG-3'; reverse: 5'-TCGTCAGTGGGAGATAGGCA-3', digesting with SphI which flanked the sgRNA target, and Sanger sequencing. Mating demonstrated that seven of the *Pcdha<sup>conex1del</sup>* mutations were on the same chromosome as the *Pcdh-g<sup>con3</sup>* allele and these lines were studied further (*Pcdh-ag<sup>f</sup>*). The *ag* deletions removed most of the *Pcdha* constant exon 1 and the subsequent exon–intron junction and splice donor site. The deletions are predicted to disrupt splicing between constant exons 1 and 2 and to cause frame shift and premature stop codons in altered exon1–intron transcripts or in exon 2 in the event of exon skipping. The above primers were used for genotyping, and distinguish the WT (756 bp) and the deleted alleles: *ag<sup>f</sup>-1*, 623 bp, corresponding to a 133bp deletion; *ag<sup>f</sup>-2*, 637 bp, corresponding to a 119 bp deletion; and *ag<sup>f</sup>-3*, 439 bp, corresponding to a 321bp deletion. The C-terminal *Pcdha* intracellular proteins encoded by constant exons 1–3 were not detected in Western blots of homozygous *ag<sup>f</sup>-1*, *ag<sup>f</sup>-2*, and *ag<sup>f</sup>-3* brain and retina tissue, confirming that the deletions disrupted *Pcdha* protein production. For the studies reported here, we used the *Pcdh-ag<sup>f</sup>* lines *ag<sup>f</sup>-1* and *ag<sup>f</sup>-3* interchangeably.

Other lines have been described previously. The *Pcdha<sup>mCherry</sup>* reporter allele, in which the *mCherry* gene is fused in frame with the *Pcdha* coding sequence at the C terminus, and the *Pcdha<sup>ko</sup>* and *Pcdhb<sup>ko</sup>* alleles, in which the entire *Pcdha* or *Pcdhb* clusters are inactivated, were described by Chen et al. (2017). The *Pcdhg<sup>con3</sup>* conditional allele contains loxP sequences flanking the third constant exon and generates a functionally null allele after Cre recombination (Lefebvre et al., 2008; Prasad et al., 2008). The *Six3-cre* line expresses Cre in retinal progenitor cells, leading to inactivation throughout the central retina, but sparing peripheral regions (<https://www.jax.org/strain/019755>; RRID:IMSR\_JAX:019755) (Furuta et al., 2000). *Chat-cre* knock-in mice express Cre in cholinergic neurons (<https://www.jax.org/strain/006410>; RRID:IMSR\_JAX:006410) (Rossi et al., 2011). SACs are the only cholinergic neurons in retina. *Pcp2-cre* has restricted activity in cerebellar Purkinje neurons (<https://www.jax.org/strain/010536>; RRID:IMSR\_JAX:010536).

Mice were maintained on a C57/B6J or mixed C57/B6-FVB background. All animal experiments were performed in accordance with Canadian Council on Animal Care Guidelines for Use of Animals in Research and Laboratory Animal Care under protocols approved by the Centre for Phenogenomics Animal Care Committee (Toronto, Canada) and National Institutes of Health guidelines and protocols approved by Institutional Animal Use and Care Committee at Harvard University.

**Histology.** Anesthetized mice were either killed by decapitation and enucleated immediately or transcardially perfused with Ringer's solution followed by 4% paraformaldehyde (PFA) in PBS. Eye cups were dissected on ice in PBS and retinas fixed in 4% PFA at 4°C (6–12 h for nuclear markers, or 2 h for antibodies to GFP or ChAT). Brains were dissected and fixed in 4% PFA at 4°C overnight.

Whole-mount preparations and cryosections of retinas were prepared as described previously (Lefebvre et al., 2008; Lefebvre et al., 2012). Briefly, retinas were cryoprotected in 30% sucrose–PBS, frozen, and sectioned at 20  $\mu\text{m}$  in a cryostat. Slides were incubated successively with blocking solution (0.35% Triton X-100, 5% normal donkey serum in PBS) and primary antibodies (12–16 h at 4°C). Whole retinas and 75  $\mu\text{m}$  sections of cerebellum were incubated successively with blocking solution and then primary antibodies for 2 d at 4°C. After washing, retinas and brain sections were incubated for 3 h at room temperature with Alexa Fluor-conjugated secondary antibodies (Thermo Fisher Scientific or Jackson ImmunoResearch). Whole retinas were flattened with photo-receptor side down onto nitrocellulose filters (Millipore).

Primary antibodies used for this study were as follows: anti-GFP (1:2000, Aves Laboratories, catalog #GFP-1010, RRID:AB\_2307313; 1:1500, Abcam, catalog #ab13970, RRID:AB\_300798); anti-choline acetyltransferase (1:250, Millipore, catalog #AB144P, RRID:AB\_2079751); anti-vesicular acetylcholine transporter (1:1000, Millipore, catalog #ABN100, RRID:AB\_2630394); anti-protein kinase Ca (1:1000, Sigma-Aldrich, catalog #P4334, RRID:AB\_477345); anti-Bassoon (1:200, Cell Signaling Technology, catalog #6897S, RRID:AB\_10828496); anti-RFP/DsRed (1:1000, Rockland, catalog #600-401-379, RRID:AB\_2209751); anti-Chx10 (1:400, Santa Cruz Biotechnology, catalog #sc-21690, RRID:AB\_2216006); anti-Sox9 (1:500, Millipore, catalog #AB5535, RRID:AB\_2239761); anti-glutamine synthetase (1:2000, BD Biosciences, catalog #610517, RRID:AB\_397879); anti-cleaved Caspase-3 (1:500, Cell Signaling Technology, catalog #9661, RRID:AB\_2341188); anti-cleaved Caspase-9 (1:300, Cell Signaling Technology, catalog #9509, RRID:AB\_2073476); anti-Brn3a (1:100, Millipore, catalog #MAB1585, RRID:AB\_94166); anti-Pax6 (1:2000, BioLegend, catalog #901301, RRID:AB\_2565003); anti-vGlut3 (1:1500, Synaptic Systems, catalog #135 203, RRID:AB\_887886); anti-synaptotagminII (1:300, DSHB, catalog #znp-1, RRID:AB\_2315626); anti-PSD95 (1:1000, Thermo Fisher Scientific, catalog #MA1-046, RRID:AB\_2092361); anti-RPBMS (1:800, PhosphoSolutions, catalog #1832-RBPMS, RRID:AB\_2492226); anti-melanopsin (1:5000, Advanced Targeting Systems, catalog #AB-N38, RRID:AB\_1608077); anti-cone arrestin (1:1000, C. Craft). Nuclei were labeled with DAPI, and cones were labeled with Alexa Fluor-647-conjugated peanut agglutinin (1:2000, Thermo Fisher Scientific, catalog #L21409, RRID:AB\_2315178).

*In situ* hybridization of retinal sections was performed as described previously (Lefebvre et al., 2008). Antisense and sense control riboprobes were synthesized using plasmid DNA templates containing cDNA sequences for the *Pcdha* constant region and 3'-UTR (Katori et al., 2009), *Pcdhg* constant region and 3'-UTR (Wang et al., 2002), and a highly conserved region of the *Pcdh-b2-b22* genes (Hirano et al., 2012).

**Western blots.** Brains or retina from postnatal day 21 (P21) to P40 and P6 mice, respectively, were dissected in ice-cold Tris-buffered saline and then homogenized in a lysis buffer containing the following: denaturing buffer (100 mM Tris-HCl, 10 mM magnesium acetate, 6 M urea, 2% SDS, w/v), EDTA-free protease inhibitors (Roche), phosphatase inhibitor cocktails I and II (Millipore), and benzonase nuclease (10 KU, Novagen). Lysates were centrifuged at 12,000 rpm for 15 min and protein concentrations were determined by BCA assay (Pierce). Equal amounts of protein (7.5  $\mu\text{g}$  for retinal lysates and 15  $\mu\text{g}$  for brain lysates) were run on a 10% SDS-PAGE gel and transferred to a polyvinylidene difluoride membrane (Millipore) overnight. Membranes were blocked for 1 h at room temperature in 1:1  $\times$  PBS and Li-Cor Odyssey Blocking Buffer and then incubated in primary antibody overnight at 4°C. The primary antibodies used for Western blot analyses were as follows:  $\alpha$ -Protocadherin (1:500, Synaptic Systems, catalog #190 003, RRID:AB\_2100951);  $\gamma$ -Protocadherin (1:750, Synaptic Systems, catalog #190 103, RRID:AB\_2100954); RFP/DsRed2 (1:1000, Rockland, catalog #600-401-379, RRID:AB\_2209751);  $\beta$ -actin (1:10,000, Cell Signaling Technology, catalog #3700, RRID:AB\_2242334); and GAPDH (1:10,000, Cell Signaling Technology, catalog #2118, RRID:AB\_561053). Membranes were washed and incubated in appropriate secondary IRDye antibodies (1:10,000, LI-COR Biosciences, catalog #926-32211, RRID:AB\_621843; and, catalog #926-68070, RRID:AB\_10956588) and visualized on a FC Odyssey Imaging System.

**RT-PCR of dissociated retina cells.** We used FACS to isolate live cells from dissociated P5–P7 whole retinas of transgenic mice, including

OPF<sup>+</sup>;Thy1.2<sup>-</sup> SAC cells and Thy1.2<sup>+</sup>; DRD4-GFP<sup>+</sup> RGCs, as described previously (Kay et al., 2012; Lefebvre et al., 2012). Using retinas from Thy1-OPF mice, OPF<sup>+</sup> SACs were sorted from OPF<sup>+</sup> RGCs by negative selection of Thy1.2-PE-Cy7 (Southern) labeled RGCs. Using retinas from DRD4-GFP<sup>+</sup> mice, a population of bistratified RGCs was sorted for GFP and Thy1.2-PE-Cy7. In each condition, 2000 cells were sorted directly into RNA lysis buffer (Qiagen). RNA was purified and first-strand cDNAs were generated with Superscript RT III (Invitrogen). *Pcdha* isoforms were amplified using primers that uniquely detect the 14 *Pcdha* variable exon-constant exon spliced transcripts (Esumi et al., 2005). The PCR program used was as follows: 94°C for 2 min; 30 cycles of 94°C for 20 s, 56°C for 30 s, 72°C for 1 min; 72°C for 7 min.

**Labeling of neurons.** To inject recombinant adeno-associated virus (AAV) into eyes, adult mice were anesthetized with isoflurane or by intraperitoneal injection of ketamine/xylazine and a 30–1/2 G needle was used to make a small hole in the temporal eye below the cornea. Then, 1.0  $\mu\text{l}$  of rAAV was injected into the subretinal space with a Hamilton syringe and 33 G blunt-ended needle, as described previously (Lefebvre et al., 2012). For cerebellar virus infection, rAAV was injected into the lateral cortical ventricle of neonates (intracerebroventricular injection), which results in the circulation of viral vectors via the CSF and transduction of neurons throughout the brain, including Purkinje cells (Passini and Wolfe, 2001). P0–P1 mice were anesthetized on ice and 1.0  $\mu\text{l}$  of viral vectors ( $\sim 2 \times 10^8$  genome copies diluted in 0.025% Fast Green in sterile PBS) were delivered in the right lateral cortical ventricle, as described previously (Lefebvre et al., 2012). Animals were killed and retinas were dissected 3–5 weeks after injection. The following recombinant vectors were used to label single SACs: AAV2/9.hEF1a.lox.TagBFP.lox.eYFP.lox.WPRE.hGH-InvBYF (Penn Vector Core, AV-9-PV2453) (Cai et al., 2013) and AAV2/2-CAG-memb-mCherry (Harvard Gene Therapy Institute). Individual Purkinje cells were transfected with: AAV8/DJ-CMV-eGFP (Vector Biolabs, 7116). AAV2/9.CAG.Flex.tdTomato.WPRE.bGH (Penn Vector Core, Allen Institute 864), AAV2/9.hSyn.HI.eGFP-Cre.WPRE.SV40 (Penn Vector Core, AV-9-PV1848). AAV.CAG.Flex.tdTomato and AAV.hSyn.HI.eGFP-Cre were coinjected to transfect and label Purkinje cells in *Pcdh-ag*<sup>fl/fl</sup> pups with Cre.

**Image analysis.** Immunofluorescence samples were imaged using a Leica SP8 confocal microscope equipped with 405, 488, 568, and 647 nm lasers. For best reproduction and clarity of SAC arborizations, maximized projections of confocal images were inverted and contrast enhanced using Photoshop (Adobe Systems) or Fiji (<http://imagej.net/Fiji/Downloads>; RRID:SCR\_002285). Modest nonlinear enhancement was applied to some representative retina images.

Measurements of retinal layer thickness and cell number were performed as described previously (Lefebvre et al., 2008). Briefly, areas of 290  $\times$  290  $\mu\text{m}$  were chosen at equivalent retinal eccentricities from the optic nerve head. Layer thickness was measured on single optical sections adjacent to the optic nerve head. Four to six areas were measured from each retina. For quantifications of ChAT-labeled SACs, four regions (290  $\times$  290  $\mu\text{m}$ ) in whole-mount retina preparations were imaged. SACs residing in the INL and GCL were quantified and combined because the two populations could not be distinguished in *Pcdh-ag*<sup>fl/fl</sup> retinas. Apoptotic cells were counted on sections spanning the optic nerve head. Cells were classified as apoptotic if immunoreactive for cleaved caspase-3 or caspase-9.

Purkinje cell dendrite self-crossings detected in single confocal planes were counted in a 70  $\times$  70  $\mu\text{m}$  region of interest located in the middle of the arbor, as described previously (Lefebvre et al., 2012). Purkinje cells from lobules 4–8 were sampled at Nyquist rates with confocal microscopy with a 0.25  $\mu\text{m}$  z-step size with a 40 $\times$  1.4 numerical aperture (NA) objective (Nikon), or 0.30–0.33  $\mu\text{m}$  z-step size and 76 nm X–Y pixel size with a 63 $\times$  1.3 NA glycerol objective (Leica). A “self-crossing” was defined when two intersecting branches were detected in the same confocal plane and both dendrites were directly apposed and contained within a maximum z-distance of 2.0  $\mu\text{m}$ , which is the combined diameter of two dendrites based on an average branch diameter of  $\sim 0.9 \mu\text{m}$  imaged with our acquisition parameters. When viewed in the orthogonal plane, the cross-sections of self-crossing dendrites could not be resolved and were displayed as continuous fluorescent structures. Overlapping branches

that were separated by several planes could be resolved as discrete cross-sections in the orthogonal plane and therefore did not meet the self-crossing criteria. The analyst was blinded to the genotypes. Self-crossing data for each genotype were compared with data from WT sibling controls and expressed as percentage of control. Purkinje arbor areas were measured using the convex-hull selection in Fiji. Arbor thickness and planarity were analyzed using the 3D volume rendering and depth coding features in the LasX 3D visualization module (Leica Microsystems); confocal images were acquired with identical z-step number and size for equivalent depth scales. WT sibling controls were used for *Pcdha*<sup>ko</sup> and *Pcdh-ag*<sup>PCKO</sup> analysis. Data for *Pcdhg*<sup>PCKO</sup> (*Pcdhg*<sup>fl/fl</sup>; Pcp2-cre and controls *Pcdhg*<sup>+/+</sup>; Pcp2-cre or *Pcdhg*<sup>+/+</sup>; Pcp2-cre) have been described previously (Lefebvre et al., 2012).

To calculate radial variance, maximum projections of SAC images were converted to a binary threshold and analyzed using the ImageJ plugin “Azimuthal Average” with a bin size of 8. Azimuthal Average calculates the average pixel intensity within a bin. SD between bins was calculated and then normalized against average pixel intensity of the entire SAC arbor to produce a unitless radial asymmetry index. Batch calculations for 17–19 neurons of each genotype were performed using Python3 script. Azimuthal Average also produces SAC radius measurements from soma edge to most distal branch point.

**Experimental design and statistical analysis.** Quantifications of cell number and neuronal morphology were performed on at least three mutant mice from multiple litters, with WT (Cre-positive and Cre-negative) or heterozygous littermates (Cre-negative) serving as controls. Animals of either sex were analyzed. The analyst was blinded to the genotypes until quantifications were complete. Statistical analyses were performed using GraphPad Prism software or Python-based statistical functions available at SciPy.org (<https://docs.scipy.org/doc/scipy/reference/stats.html>). All data are presented as means with SEMs unless otherwise stated. Means of two groups were compared using the two-tailed Student's *t* test on condition of equivalent variances determined by the ANOVA *F* test, or with the Mann–Whitney nonparametric test. Means of multiple samples were compared using one-way ANOVA and Tukey's multiple-comparisons test for pairwise analyses. Exact *p*-values are reported unless the values are <0.0001.

## Results

### Differential and overlapping expression of *Pcdh-α*, *Pcdh-β*, and *Pcdh-γ* clusters in retina

We reported previously that *Pcdhgs* are expressed by all retinal cell types: photoreceptors in the ONL; interneurons (horizontal, bipolar, and amacrine cells) and Müller glia in the INL; and amacrine and RGCs in the GCL (Lefebvre et al., 2008). To begin this study, we assessed expression of *Pcdhas* and *Pcdhbs* in retina and compared their expression patterns with that of *Pcdhgs*. We designed *in situ* hybridization riboprobes targeting the constant exons shared by all *Pcdha* or *Pcdhg* isoforms or a highly conserved sequence present in the majority of *Pcdhb* isoforms (Fig. 1A) (Hirano et al., 2012). *Pcdha*, *Pcdhb*, and *Pcdhg* mRNAs were all expressed broadly in the INL and GCL at P6 (Fig. 1B), a time at which many neurons die and dendritic self-avoidance fails in *Pcdhg* mutants (Lefebvre et al., 2008; Lefebvre et al., 2012). However, *Pcdha* mRNA was relatively more abundant in the GCL than in the INL compared with *Pcdhb* and *Pcdhg*, a pattern that persisted at P14, after inner retinal development is mostly complete.

To map *Pcdha* expression in greater detail, we used a *Pcdha*<sup>mCherry</sup> reporter line in which mCherry is fused to the final constant *Pcdha* exon within the endogenous locus, producing *Pcdha* proteins tagged at the carboxy terminus of the common cytoplasmic domain (Chen et al., 2017). This line is similar in design to the *Pcdhg*<sup>GFP</sup> line that we used previously to map *Pcdhg* expression (Wang et al., 2002; Lefebvre et al., 2008). The reporter confirmed the expression of *Pcdhas* in RGCs and in SACs in which *Pcdhgs* are required for dendritic self-avoidance (Fig. 1C–E). Neither of

these approaches distinguished between the expression of the 12 alternate or the two C-type *Pcdha* variants, which diverge in sequence identity and gene regulatory mechanisms (Wu and Maniatis, 1999; Wu et al., 2001; Esumi et al., 2005). We therefore profiled *Pcdha* isoforms by RT-PCR of RNA obtained from whole P7 retina or genetically labeled retinal subpopulations purified by FACS. Both alternate and C-type *Pcdha* isoforms were expressed by retinal cells, including bipolar cells, RGCs and SACs (Fig. 1F and data not shown).

### *Pcdha* and *Pcdhb* clusters are dispensable for retinal cell survival

We next investigated whether *Pcdhas* or *Pcdhbs* are required for retinal development. We compared retinas from single-cluster *Pcdha* and *Pcdhb* knock-out mice (*Pcdha*<sup>ko</sup>, *Pcdhb*<sup>ko</sup>; Chen et al., 2017), which are viable and fertile, with retinas in which *Pcdhgs* were conditionally deleted with a pan-retinal Cre (*Pcdhg*<sup>fl/fl</sup>; *Six3-cre*, referred to as *Pcdhg*<sup>trko</sup> for retina-specific knock-out). We detected no abnormalities in retinal architecture in *Pcdha*<sup>ko</sup> and *Pcdhb*<sup>ko</sup> lines and the density of synapses in the plexiform layers appeared normal as judged by staining with antibodies to Bassoon, a presynaptic marker associated with neurotransmitter release sites in nerve terminals (Fig. 2A). Moreover, in contrast to thinning of the inner retinal layers in *Pcdhg*<sup>trko</sup>, the thickness of the INL and the IPL in *Pcdha*<sup>ko</sup> and *Pcdhb*<sup>ko</sup> mutant retinas were similar to those in controls (Fig. 2A; quantification for *Pcdha*<sup>ko</sup> in Fig. 2J). We used Western blotting to determine whether upregulation of *Pcdhgs* could compensate for the loss of *Pcdhas*, but found no change in *Pcdhg* protein levels in *Pcdha*<sup>ko</sup> mutant retinas (Fig. 2B). Therefore, in contrast to *Pcdhg*, the *Pcdha* and *Pcdhb* gene clusters are dispensable for major aspects of retinal development, including neuronal generation and survival.

### Inactivation of both the *Pcdha* and *Pcdhg* clusters results in a synergistic loss of inner retinal layers

*Pcdha*, *Pcdhb*, and *Pcdhg* genes are expressed in overlapping populations of retinal cells and the proteins that they encode are highly homologous. Therefore, although *Pcdha* or *Pcdhb* deletion alone did not have a striking retinal phenotype, functional compensation by the *Pcdhgs* might mask their roles. To test this possibility, we set out to generate a mouse mutant lacking multiple *Pcdh* clusters. Deletion of the three *Pcdh* clusters is complicated by the locus size (1 MB; Wu and Maniatis, 1999) and the presence of the *Taf7* gene, which encodes a component of the transcription machinery, between the *Pcdhb* and *Pcdhg* clusters. *Taf7* mutants die between embryonic days 3.5 and 5.5 (Gegonne et al., 2012; Hasegawa et al., 2016). Accordingly, triple cluster *Pcdh* mutant mice require transgenic restoration of the *Taf7* gene to develop to term (Hasegawa et al., 2016; Mountoufaris et al., 2017). Even with *Taf7* restored, triple cluster mice die soon after birth, likely due to the neonatal lethality caused by constitutive deletion of *Pcdhg* (Wang et al., 2002). To circumvent this limitation, we used the Crispr-Cas9 system to mutate *Pcdha* in the conditional *Pcdhg*<sup>fl</sup> floxed allele (Lefebvre et al., 2008), choosing *Pcdha* over *Pcdhb*, because it has been studied in greater detail (Lefebvre, 2017). We used an sgRNA designed to target the *Pcdha* constant exon 1 because, in our previous studies, targeting of a constant exon in the *Pcdhg* locus generated a null allele (Wang et al., 2002; Lefebvre et al., 2008; Prasad et al., 2008). The sgRNA and Cas9 were injected into *Pcdhg*<sup>f</sup> zygotes to generate *Pcdha*<sup>conex1del</sup>; *Pcdhg*<sup>f</sup> mice, hereafter called *Pcdh-ag*<sup>f</sup> (Fig. 2C).

We chose three *Pcdh-ag*<sup>f</sup> founders with deletions of >100 bp spanning the exon–intron site that are predicted to disrupt splic-

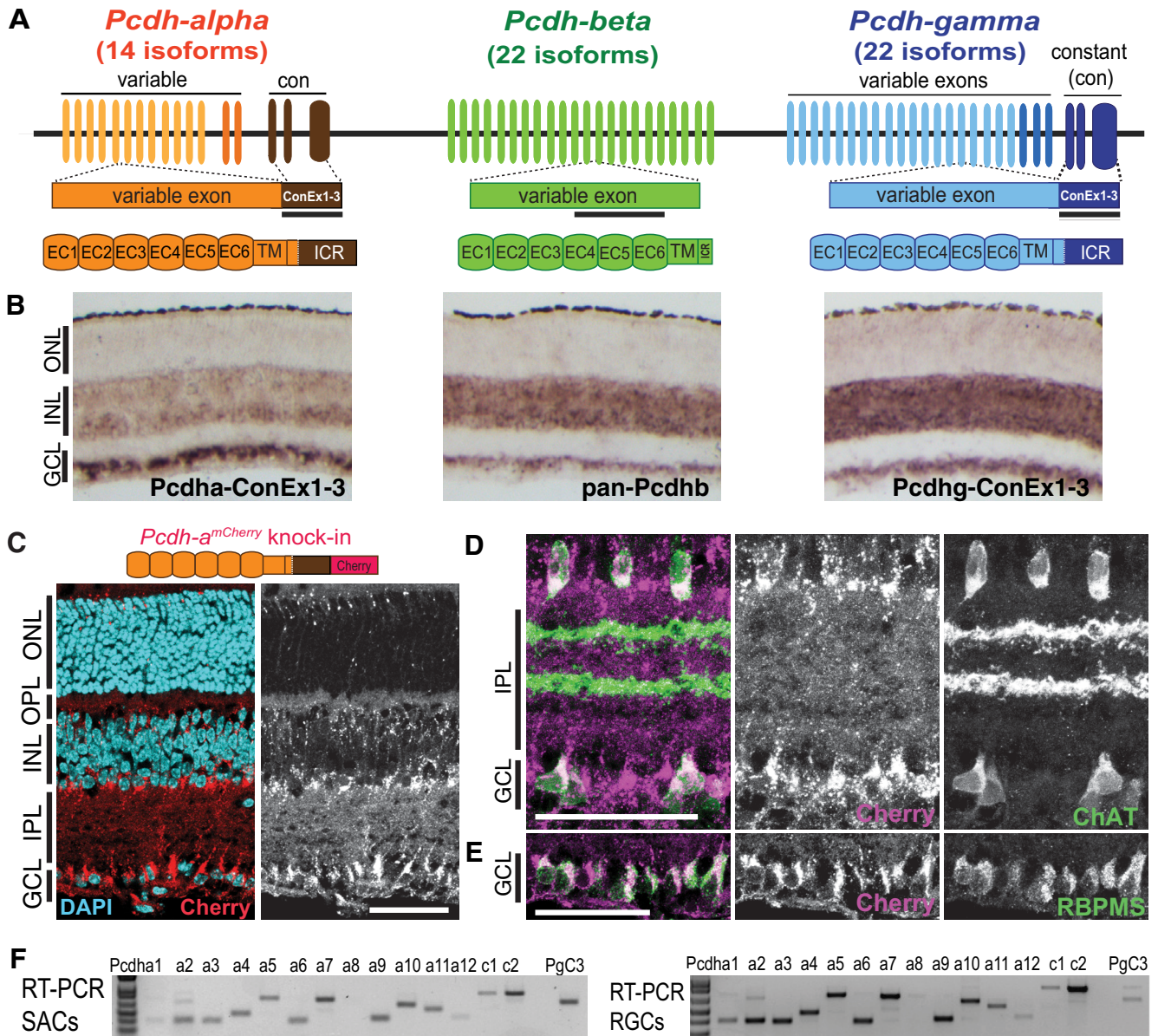


**Figure 1.** Expression of the clustered protocadherins in mouse retina. **A**, Schematic representation of the *Pcdh* locus comprising the *Pcdha*, *Pcdhb*, and *Pcdhg* clusters. *Pcdha* and *Pcdhg* mRNAs are assembled by splicing a variable exon to three constant exons (ConEx 1–3). Each variable exon is transcribed from its own promoter. Black bars represent region targeted by *in situ* hybridization riboprobes. Bottom, *Pcdha*, *Pcdhb*, and *Pcdhg* isoforms share similar protein organization, including six extracellular calcium motifs (EC), one transmembrane domain, and an intracellular region (ICR). **B**, *In situ* hybridization of P7 retinas showing *Pcdha*, *Pcdhb*, and *Pcdhg* mRNA expression in the INL and the GCL. **C–E**, *Pcdha* expression revealed by a *Pcdha*-mCherry fusion protein (**C**, top) generated by insertion of mCherry at the 3' end of the *Pcdha* coding region in the endogenous locus. Sections from P14 retinas show expression of *Pcdha*-mCherry proteins in the INL and GCL (**C**, red, with DAPI in cyan). Costaining with antibodies to mCherry confirm expression of *Pcdhas* in SACs (**D**, ChAT, green), and RGCs (**E**, RBPMS, green). **F**, RT-PCR of alternate (a1–a12) and C-type (c1, c2) *Pcdha* transcripts from RNA extracts of SACs and a subpopulation of RGCs purified by FACS. Scale bars, 50  $\mu$ m.

ing and alter the protein coding sequence for the *Pcdha* intracellular domain (Fig. 2C). Using an antibody targeting the constant region, we confirmed the absence of full-length *Pcdha* proteins in *Pcdha-ag<sup>fl/fl</sup>* brain lysates (Fig. 2D). Due to lack of available antibodies that recognize *Pcdha* ectodomains, we could not test for the presence of truncated *Pcdha* proteins. Therefore, we investigated whether our mutants displayed a previously documented effect of *Pcdha* deletion on the clumping and disorganization of serotonergic axons in the hippocampus (Katori et al., 2009; Chen et al., 2017). Defects in serotonergic projections were similar in *Pcdha-ag<sup>fl/fl</sup>* homozygotes, *Pcdha<sup>ko/ko</sup>* homozygotes, and *Pcdha<sup>ko</sup>*; *Pcdha-ag<sup>f</sup>* transheterozygotes (data not shown), confirming that the Crispr-mediated deletions effectively disrupted *Pcdha* func-

tion. In subsequent experiments, we used two lines, *Pcdha-ag<sup>f-1</sup>* and *Pcdha-ag<sup>f-3</sup>*, interchangeably; results from the two were indistinguishable.

We expected that *Pcdha-ag<sup>fl/fl</sup>* mice would be equivalent to *Pcdha<sup>ko/ko</sup>* in the absence of Cre and therefore viable. We were therefore surprised to recover few *Pcdha-ag<sup>fl/fl</sup>* mutant animals from crosses between *Pcdha-ag<sup>fl/fl</sup>* mice. Moreover, compared with WT littermates, *Pcdha-ag<sup>fl/fl</sup>* mice were smaller and exhibited a hunched posture, stiffness, and limb tremors (Fig. 2E). These phenotypes resemble those of *Pcdhg<sup>ko</sup>* neonates and are thought to result from an excessive neuronal loss in the spinal cord and brainstem (Wang et al., 2002; Hasegawa et al., 2017). Surviving *Pcdha-ag* animals were also smaller at the time of weaning (Fig. 2F;

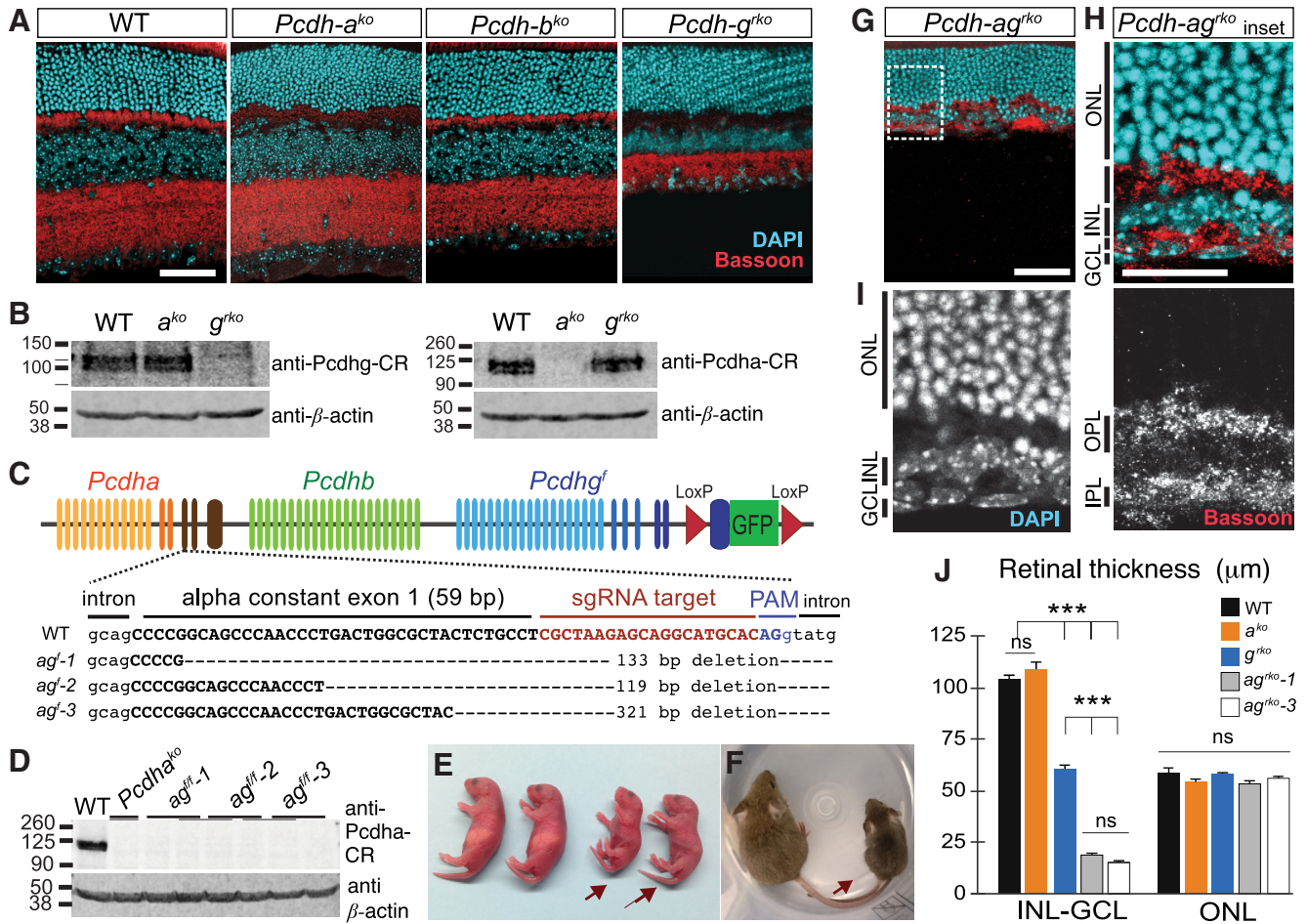


**Figure 2.** Synergistic loss of inner retinal structures in *Pcdh-ag* double mutant retinas. **A**, Retina sections from WT, *Pcdha*<sup>ko</sup>, *Pcdhb*<sup>ko</sup>, and *Pcdhg*<sup>rko</sup> animals labeled with anti-Bassoon (red) to mark synapses and DAPI (cyan) to mark cells. **B**, Western blots of *Pcdha* and *Pcdhg* proteins in *Pcdha*<sup>ko</sup> and *Pcdhg*<sup>rko</sup> retinas using antibodies to the constant region (CR) shared by all isoforms in each cluster. **C**, CRISPR/Cas9 targeting of *Pcdha* constant exon 1 (capital letters) in *Pcdhg*<sup>f</sup> allele. Three *Pcdh-ag*<sup>f</sup> founders with deletions spanning exon–intron junction: *ag*<sup>f-1</sup>, *ag*<sup>f-2</sup>, and *ag*<sup>f-3</sup>. **D**, Western blots of *Pcdha* in brain lysates of WT, *Pcdha*<sup>ko</sup>, *ag*<sup>f-1</sup>, *ag*<sup>f-2</sup>, and *ag*<sup>f-3</sup> animals. **E, F**, *Pcdh-ag*<sup>f/f</sup> animals (arrows) are smaller than littermate controls at P0 (**E**) and P21 (**F**). **G**, *Pcdh-ag*<sup>rko</sup> retina labeled with anti-Bassoon (red) and DAPI (cyan). **H, I**, Higher magnification of boxed region in **G, J**. Comparisons of inner retina (INL, IPL, and GCL combined) and outer retina (ONL) thickness in single and double *Pcdh* mutant retinas. *Pcdh-ag*<sup>rko</sup> retinas from *ag*<sup>f-1</sup> and *ag*<sup>f-3</sup> lines have similar reductions (ns, not significant, *p* = 0.62, *post hoc* Tukey test). Data show mean ± SEM. *n* = 18 sections from 3–5 animals per genotype. INL: one-way ANOVA, *F*<sub>(4,85)</sub> = 6.4, *p* < 0.0001; pairwise Tukey’s multiple-comparisons tests, \*\*\**p* < 0.0001. ONL: one-way ANOVA, *F*<sub>(4,85)</sub> = 2.4, *p* = 0.071; pairwise Tukey’s multiple-comparisons tests, not significant (ns). Scale bars: **A, G**, 50 μm; **H**, 25 μm.

controls = 12.0 ± 0.5 g; *Pcdh-ag*<sup>f/f</sup> = 6.9 ± 0.6 g, *n* = 13 animals, *t*<sub>(24)</sub> = 8.0, *p* < 0.0001, unpaired *t* test). The likely explanation is that the targeted *Pcdhg*<sup>f</sup> allele, even in the absence of Cre, is hypomorphic (Lefebvre et al., 2008; Prasad et al., 2008). Therefore, although *Pcdhg*<sup>f/f</sup> animals are viable and fertile, decreased levels of Pcdhgs in *Pcdh-ag*<sup>f</sup> would lead to decreased viability. This result provided an initial indication that postnatal viability is affected by interactions between Pcdhas and Pcdhgs.

To seek retinal phenotypes, we crossed *Pcdh-ag*<sup>f</sup> mice to a Six3-cre line that is expressed in retinal progenitors to limit *Pcdhg* deletion to retina and analyzed survivors (*Pcdh-ag*<sup>f/f</sup>; *Six3-cre*, referred to as *Pcdh-ag*<sup>rko</sup>, *rko* indicating pan-retinal and retina-specific knock-out). We avoided use of *Pcdh-ag*<sup>f/f</sup> mice as controls, instead using Cre-positive or Cre-negative WT mice or Cre-negative *Pcdhg*<sup>f/f</sup> littermates. At P21, when retinal architecture is fully developed in controls, the inner retina was nearly eliminated in *Pcdh-ag*<sup>rko</sup> mice. All retinal layers were present, but the INL and IPL were dramatically thinned (Fig. 2G). The INL contained only a few layers of cells, whereas the IPL was reduced to a thin layer of processes (Fig. 2H, I). Remarkably, the ONL comprising the photoreceptors remained intact. We measured the combined

thickness of the inner retinal layers (INL, IPL, and GCL). Compared with the inner retinal layers in *Pcdha*<sup>ko</sup> retinas (unchanged, 108.8 ± 3.3 μm compared with WT control 103.9 ± 1.9 μm, *p* = 0.35, Tukey’s pairwise comparison) and in *Pcdhg*<sup>rko</sup> retinas (reduced by 40%, 60.9 ± 1.4 μm), the layers were reduced by >80% in double *Pcdh-ag*<sup>rko</sup> mutant retinas (*ag*<sup>rko</sup> line 1: 18.6 ± 0.6 μm; *ag*<sup>rko</sup> line 3: 15.4 ± 0.5 μm; *n* = 18 sections, from 3–5 animals per genotype, one-way ANOVA *F*<sub>(4,85)</sub> = 6.4, *p* < 0.0001; Tukey’s multiple-comparisons test between *ag*<sup>rko</sup> lines and single *Pcdh* mutants, *p* < 0.0001; Fig. 2J). In contrast, the thickness of the OPL was unaffected. Therefore, Pcdhas and Pcdhgs act synergistically to form or maintain the inner retina.

**Developmental cell death of inner retinal neurons in *Pcdh-ag*<sup>rko</sup> mutant retinas**

We next investigated whether retina thinning in *Pcdh-ag*<sup>rko</sup> mutants results from reduced numbers of inner retinal neurons. Numbers of bipolar cells (Chx10+), amacrine cells (Pax6+), and RGCs (Brn3a+) were unaffected in single *Pcdha*<sup>ko</sup> retina, consistent with results presented above, but reduced far more in double *Pcdh-ag*<sup>rko</sup> than in single *Pcdhg*<sup>rko</sup> retina: ~80% and 72% reduc-

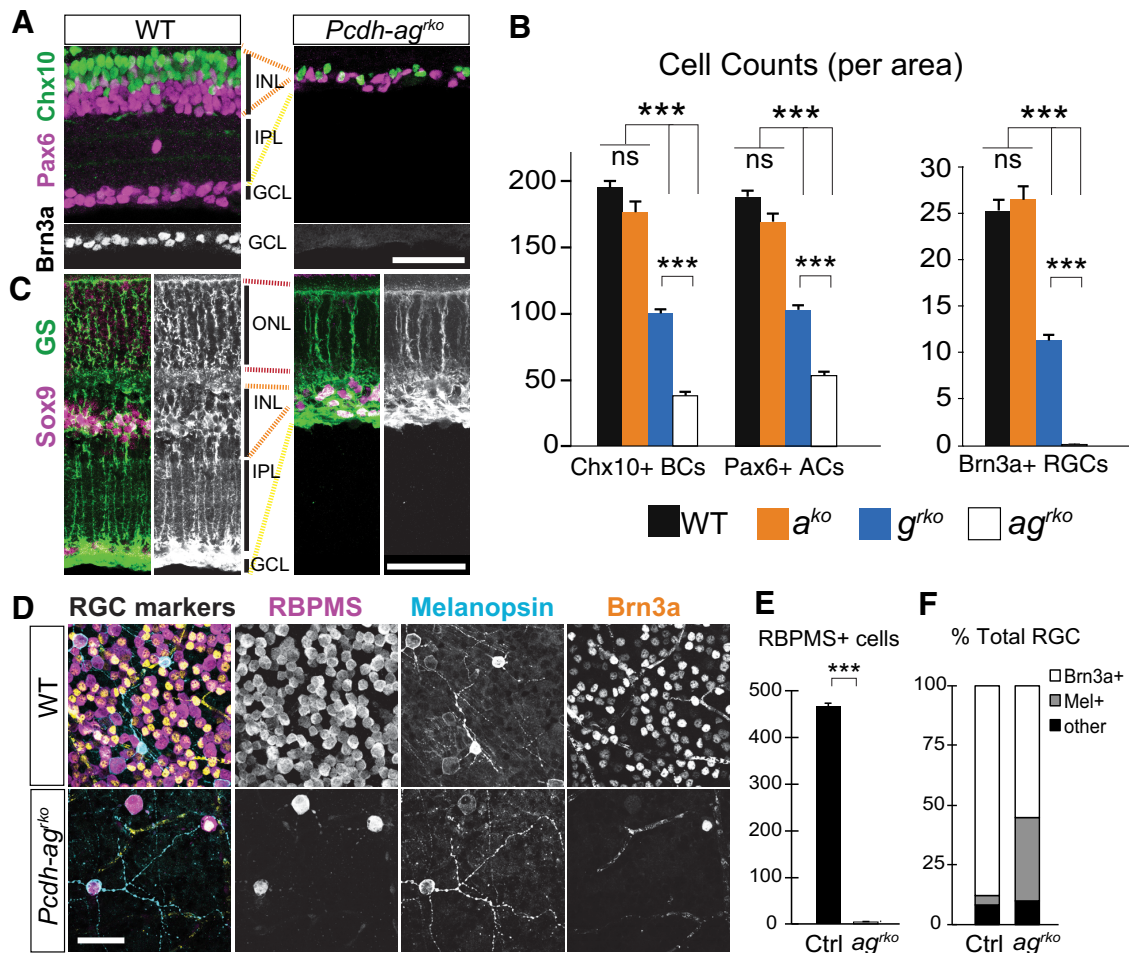


**Figure 3.** Synergistic loss of interneurons and RGCs in *Pcdh-ag* double mutant retinas. **A–C**, Sections of P21 WT and *Pcdh-ag*<sup>rko</sup> retinas immunostained for retinal cell markers. **A**, Chx10+ bipolar cells (BC, green), Pax6+ amacrine cells (AC, magenta), and Brn3a+ RGCs (white) in WT and *Pcdh-ag*<sup>rko</sup> retinas. **B**, Quantifications of BCs, ACs, and RGCs in *Pcdh*<sup>rko</sup>, *Pcdhg*<sup>rko</sup>, and *Pcdh-ag*<sup>rko</sup> retina sections from 4–6 animals per genotype. Chx10 counts: one-way ANOVA,  $F_{(3,76)} = 217.3, p < 0.0001, n = 20$  sections. Tukey’s multiple-comparisons tests,  $p < 0.0001$ . Pax6 counts: one-way ANOVA,  $F_{(3,76)} = 260.3, p < 0.0001, n = 20$  sections. Brn3a counts: one-way ANOVA,  $F_{(3,60)} = 165.1, p < 0.0001, n = 16$  sections. **C**, Müller glia immunolabeled for glutamine synthetase (green) and Sox9 (magenta). **D–F**, Analysis of RGC survival in *Pcdh-ag*<sup>rko</sup> and WT whole-mount retinas. **D**, Immunostaining with RGC markers (RBPMS, magenta; melanopsin, cyan; Brn3a, yellow). **E**, Counts of cells labeled with antibodies to RBPMS, a pan-RGC marker.  $n = 12$  retina sections, 3 animals per genotype,  $p < 0.0001$ , Mann–Whitney *U* test. **F**, Analysis of two mutually exclusive Brn3a+ and Mel+ RGC populations expressed as percentage total RGCs among surviving RGCs in *Pcdh-ag*<sup>rko</sup> retinas. Data are shown as means  $\pm$  SEM. \*\*\* $p < 0.0001$ . Scale bars, 50  $\mu$ m.

tions for bipolars and amacrine cells in *Pcdh-ag*<sup>rko</sup>, respectively, compared with ~50% and 45% in *Pcdhg*<sup>rko</sup> mutants (Fig. 3*A,B*; Chx10,  $n = 20$  sections: one-way ANOVA,  $F_{(3,76)} = 217.3, p < 0.0001$ ; Pax6,  $n = 20$  sections: one-way ANOVA,  $F_{(3,76)} = 260.3, p < 0.0001$ ; Tukey’s multiple-comparisons test,  $p < 0.0001$  between genotypes, except for the WT and *Pcdha*<sup>rko</sup> pair). Most dramatically, only 1% of RGCs persisted in *Pcdh-ag*<sup>rko</sup> retina (one-way ANOVA,  $F_{(3,60)} = 165.1, p < 0.0001$ ; Tukey’s multiple-comparisons test,  $p < 0.0001$  between genotypes, except for the WT and *Pcdha*<sup>rko</sup> pair,  $p = 0.85$ ). Müller glia cells were also reduced in number but maintained processes spanning the retina (Fig. 3*C*). Photoreceptors were spared in both *Pcdh-g*<sup>rko</sup> retinas (Fig. 2*A,J*; Lefebvre et al., 2008) and *Pcdh-ag*<sup>rko</sup> retinas (Fig. 2*G,J*).

We stained retinal whole mounts to characterize the few surviving RGCs in *Pcdh-ag*<sup>rko</sup> mutants. Examination of the entire RGC population with a pan-RGC marker confirmed their near elimination, with a mere 1.1% of RGCs remaining in *Pcdh-ag*<sup>rko</sup> retinas compared with controls ( $n = 12$  retina sections, 3 animals per genotype,  $p < 0.0001$ , Mann–Whitney *U* test; Fig. 3*D,E*). We next quantified two mutually exclusive RGC cell types, the Brn3a+ RGCs and the melanopsin-positive intrinsically photo-

sensitive RGCs (Mel+ ipRGCs) (Rodriguez et al., 2014). Both surviving RGC subpopulations are sparse, but proportionally more Mel+ ipRGCs remained in mutant *Pcdh-ag*<sup>rko</sup> retinas (4.1% of total RGCs are Mel+ in control compared with 35% of Mel+/total RGCs in *Pcdh-ag*<sup>rko</sup> mutants; Fig. 3*D–F*). The enrichment of Mel+ ipRGCs among surviving RGCs indicates a resistance to cell death, which has also been observed for ipRGC subpopulations in injury models such as axotomy and optic neuropathies (Pérez de Sevilla Müller et al., 2014; Cui et al., 2015; Duan et al., 2015).

We also examined retinas at earlier and later times to determine when *Pcdh* act. RGCs and amacrine cells were present in *Pcdh-ag*<sup>rko</sup> mutant retinas at P0 but had severely declined in number by P6 (Fig. 4*A–D*). RGCs were already eliminated by this time, revealing the rapid loss of RGCs within the first postnatal days (Fig. 4*C,D*). During this time, populations of inner retinal cells are reduced by a stereotyped wave of developmental cell death (Young, 1984). In *Pcdh-ag*<sup>rko</sup> mutant retinas, more apoptotic cells were detected in mutant than in control INL at P6 by staining for cleaved-caspase 9 and cleaved-caspase 3 (Fig. 4*E,F*), indicating that loss of retinal cells occurs from accentuated cell death ( $n = 18$  sections, 4–5 animals per genotype; CC3,  $p = 0.0051$ ; CC9,  $p = 0.0010$ , Mann–Whitney test). These data support the idea documented pre-

viously for Pcdhgs that Pcdhs promote neuronal survival rather than attenuating neurogenesis (Lefebvre et al., 2008). Defects in *Pcdh-ag<sup>rko</sup>* mutant retinas were not detectably more severe at P70 than at P21, further indicating that cell loss is developmentally restricted (Fig. 4*G,H*). Together, these results demonstrate that *Pcdha* and *Pcdhg* act synergistically and redundantly to promote survival of retinal neurons during early postnatal life.

#### Degraded sublaminal organization of plexiform layers in *Pcdh-ag<sup>rko</sup>* mutant retinas

A key feature of retinal circuit organization is that axons and dendrites of specific neuronal types are restricted to one or a few of ~10 sublaminae within the IPL and one of two sublaminae within the OPL, thus constraining their choice of synaptic partners (Sanes and Zipursky, 2010; Lefebvre et al., 2015). We showed previously that Pcdhgs are dispensable for sublamina-specific arborization of processes in the IPL and OPL (Lefebvre et al., 2008) and used similar methods to show that sublaminal organization persists in *Pcdha<sup>rko</sup>* retina (data not shown). We investigated whether this preservation reflects redundant functions of Pcdhas and Pcdhgs. In the IPL, processes of OFF and ON bipolar subtypes are segregated to distal and proximal IPL sublayers, respectively. Sections were double labeled with antibodies to Syt2, which labels Type 2 OFF cone bipolars, and to protein kinase C $\alpha$ , which labels ON rod bipolars. Axon terminals labeled by these markers were clearly segregated in control retina but were intermingled in *Pcdh-ag<sup>rko</sup>* retina (Fig. 5*A,B*). We also labeled two amacrine cell types: SACs with antibodies to choline acetyltransferase (ChAT) and a narrow-field subtype with vGluT3. In control, the two SAC populations residing in the INL and in the GCL form two segregated dendritic layers in the IPL, whereas the vGluT3+ amacrine cells form processes between them (Fig. 5*C*). In *Pcdh-ag<sup>rko</sup>* retinas, this segregation was lost as the narrow ChAT+ bands collapsed (Fig. 5*D*). Moreover, nearly all vGluT3+ amacrine cells were absent.

In the OPL, synapses of rod terminals (spherules) on rod bipolar dendrites are concentrated in an outer sublamina, abutting the ONL, whereas synapses of cone terminals (pedicles) on cone bipolar dendrites occupy an inner sublamina, abutting the INL (Fig. 5*E*). This sublaminal organization was also disrupted in *Pcdh-ag<sup>rko</sup>* retina, with rod spherules and cone pedicles intermixed (Fig. 5*F*). Cone photoreceptor morphology was intact in mutants (Fig. 5*F*) but PNA labeling revealed fragmentation at the base of cone pedicles, suggesting disorganized contacts with postsynaptic partners (Fig. 5*G*). Therefore, the combined loss of the *Pcdha* and *Pcdhg* clusters has devastating consequences on

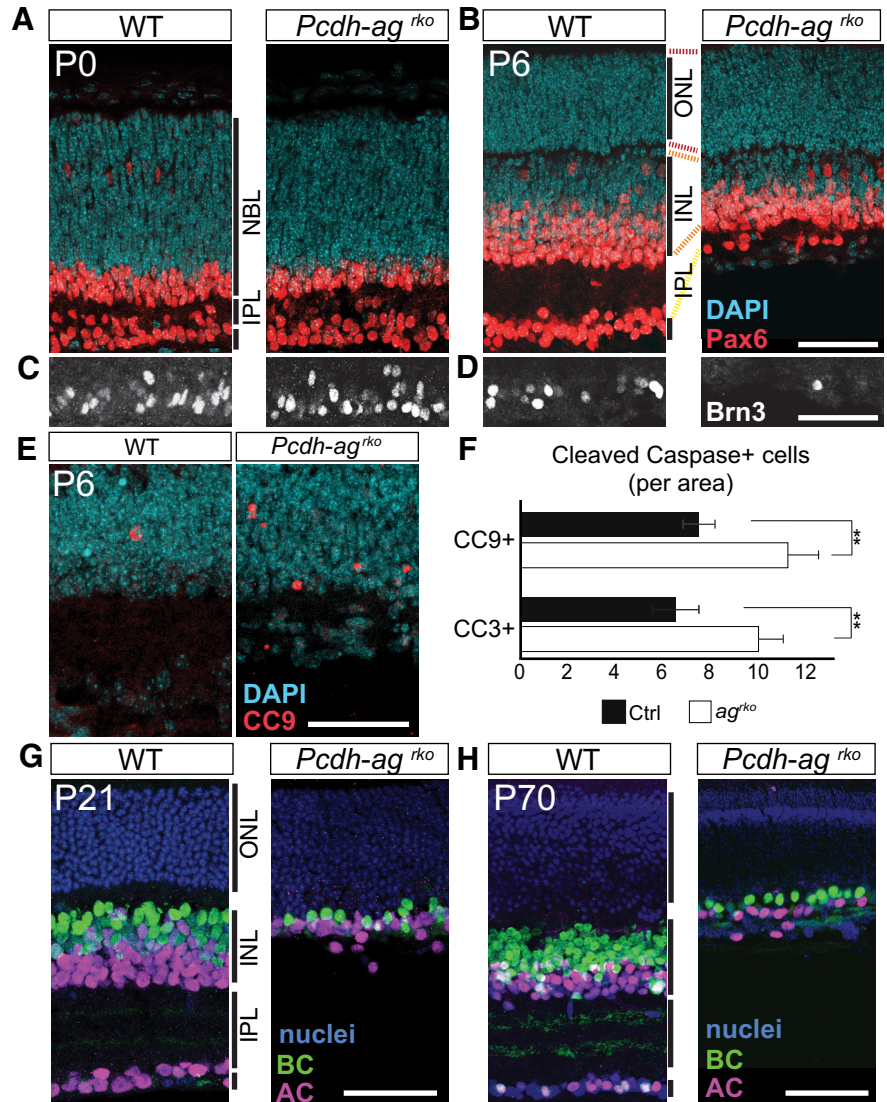


**Figure 4.** Retinal cell loss from accentuated postnatal cell death in double *Pcdh-ag* mutant retinas. **A–D**, Immunolabeling of ACs (Pax6+, red; **A, B**) and RGCs (Brn3c+, white; **C, D**) reveal decline in RGC and AC populations in *Pcdh-ag<sup>rko</sup>* retinas from P0 (**A, C**) to P6 (**B, D**) compared with WT. NBL, neuroblastic layer. **E**, Apoptotic cells marked by cleaved caspase-9 (CC9) in control and *Pcdh-ag<sup>rko</sup>* retinas at P6. **F**, Quantifications of CC9- and cleaved caspase-3-positive cells confirmed increased apoptosis in *Pcdh-ag<sup>rko</sup>* retinas. Data show mean  $\pm$  SEM from 4–5 animals per genotype. CC3:  $p = 0.0051$ , Mann–Whitney  $U$  test,  $n = 18$  sections. CC9:  $p = 0.001$ , Mann–Whitney  $U$  test,  $n = 18$  sections.  $**p < 0.01$ . **G, H**, Comparisons of AC and BC populations in *Pcdh-ag<sup>rko</sup>* retinas at P21 and P70 show that inner retina cell loss is not progressive with age. **G**, Anti-Pax6 is shown in magenta; anti-Chx10 in green, and DAPI in blue. **H**, Anti-AP2 is shown in magenta; anti-Chx10 in green, and TO-PRO in blue. Dashed lines indicate retinal layers. Scale bars, 50  $\mu$ m.

many aspects of IPL and OPL development. Disruptions to sublaminal organization may be in part a consequence of neuronal loss. For example, the number of bipolar cells is reduced by ~80% (Fig. 3*B*) and vGluT3+ amacrine cells are almost completely eliminated in *Pcdh-ag<sup>rko</sup>* retina (Fig. 5*D*). Alternatively, Pcdhs may mediate interactions among processes required for their segregation. At present, we cannot distinguish between these possibilities.

We examined neonatal retinas to determine whether IPL lamination was disrupted from the outset or degraded during development. Little bipolar stratification occurs until the second postnatal week, but SACs form lamina-restricted arbors in neonates. Processes of SACs were laminated similarly in control and *Pcdh-ag<sup>rko</sup>* retinas at P0 but had collapsed by P6 (Fig. 5*H*). These

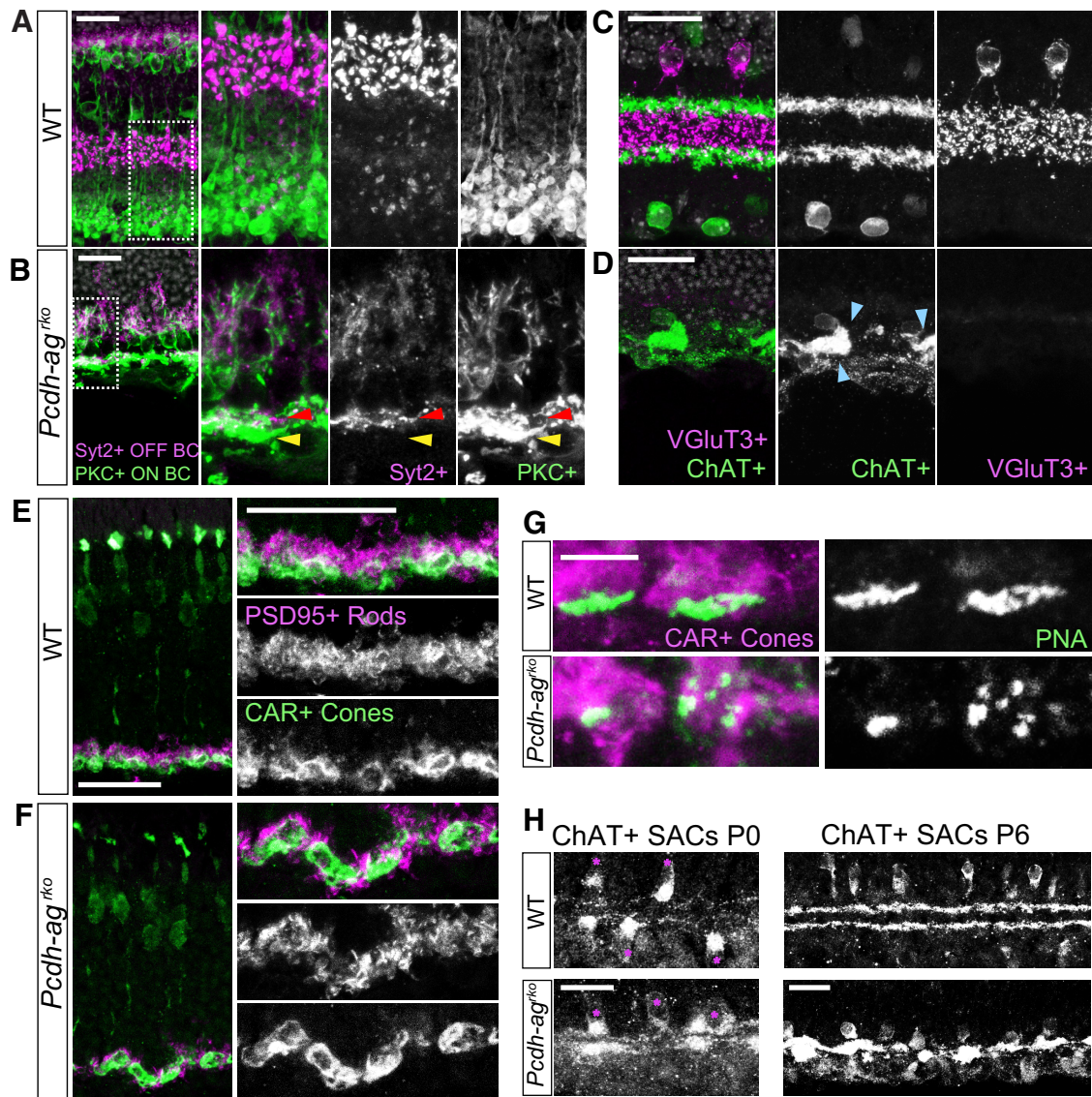


**Figure 5.** Laminal organization of the IPL and OPL is not maintained in the absence of *Pcdha* and *Pcdhg* clusters. **A, B**, Sections of inner retina showing laminar segregation of OFF cone bipolar (Syt2+, magenta) and ON rod bipolar axon terminals (PKC $\alpha$ +, green) in IPL of P21 WT (**A**) and *Pcdh-ag*<sup>rko</sup> retinas (**B**). White boxes in left panels indicate regions shown at higher magnification in the other panels. Arrows indicate OFF (red) and ON (yellow) BC terminals, which are intermingled in *Pcdh-ag*<sup>rko</sup>. **C, D**, Laminal segregation of AC processes: vGluT3+ narrow field ACs (magenta) form elaborate processes between two ChAT+ SAC layers (green) in WT (**C**) at P21. In *Pcdh-ag*<sup>rko</sup> retinas (**D**), vGluT3+ ACs are absent and ChAT+ layers are collapsed. Blue arrows denote clumping of SAC dendrites. **E, F**, Sections of outer retina showing laminar organization of rod (PSD95+, magenta) and cone (CAR+, green) terminals in OPL. **E**, WT. **F**, Rod spherules are displaced relative to cone pedicles in *Pcdh-ag*<sup>rko</sup>. **G**, Lectin PNA labeling show fragmentation of cone synaptic structures in *Pcdh-ag*<sup>rko</sup> retinas. **H**, SAC processes are stratified in WT and *Pcdh-ag*<sup>rko</sup> retina at P0 (left), but are collapsed in *Pcdh-ag*<sup>rko</sup> retina at P6 (right). Scale bars: **A–F**, 25  $\mu$ m; **G**, 5  $\mu$ m.

data demonstrate that IPL disruption in double *Pcdh* mutants becomes more pronounced during postnatal development.

#### Dose-dependent requirement for *Pcdhas* and *Pcdhgs*

To investigate systematically the relative contributions of *Pcdhas* and *Pcdhgs* to retinal development, we analyzed *Pcdh* gene cluster dosage in a series of mutant retinas lacking one or both copies of the *Pcdha* or *Pcdhg* clusters. For example, we crossed *Pcdh-ag*<sup>rko/+</sup> to *Pcdh-a*<sup>ko</sup> mice to generate *Pcdh-a*<sup>rko/ko</sup>; *g*<sup>rko/wt</sup> retinas (abbreviated here as *Pcdh-a*<sup>0</sup>*g*<sup>1</sup>, in which *a*<sup>0</sup> denotes no WT *Pcdha* allele and *g*<sup>1</sup> denotes one WT *Pcdhg* allele) and *Pcdh-ag*<sup>rko/+</sup> to *Pcdh-g*<sup>rko</sup> mice to generate *Pcdh-a*<sup>rko/wt</sup>; *g*<sup>rko/rko</sup> retinas (*Pcdh-a*<sup>1</sup>*g*<sup>0</sup>). Overall, the series included retinas from seven genotypes with decreasing cluster dosage: four (*Pcdh-a*<sup>2</sup>*g*<sup>2</sup>), two

(*Pcdh-a*<sup>1</sup>*g*<sup>1</sup>, *Pcdh-a*<sup>0</sup>*g*<sup>2</sup>, *Pcdh-a*<sup>2</sup>*g*<sup>0</sup>), one (*Pcdh-a*<sup>1</sup>*g*<sup>0</sup>, *Pcdh-a*<sup>0</sup>*g*<sup>1</sup>), or zero (*Pcdh-a*<sup>0</sup>*g*<sup>0</sup>) *Pcdha* or *Pcdhg* alleles (Fig. 6A).

To quantify the degree of cell loss in this allelic series, we measured the thickness of the inner retina (INL, IPL, and GCL combined) and the numbers of bipolar, amacrine, and RGCs, expressing each as a percentage of the value quantified in littermates. Cell loss was exquisitely sensitive to *Pcdh* dosage, revealing cluster-specific and dose-dependent survival activities of *Pcdhs* (Fig. 6A–E). When both copies of the *Pcdha* cluster were deleted, a single WT copy of *Pcdhg* was insufficient to support survival: the numbers of bipolar cells and RGCs were significantly reduced in *Pcdh-a*<sup>0</sup>*g*<sup>1</sup> retinas compared with control retinas (by 18% and 32%, respectively;  $p < 0.0001$ , *post hoc* Tukey pairwise test). However, a single copy of the *Pcdha* cluster was able to compen-

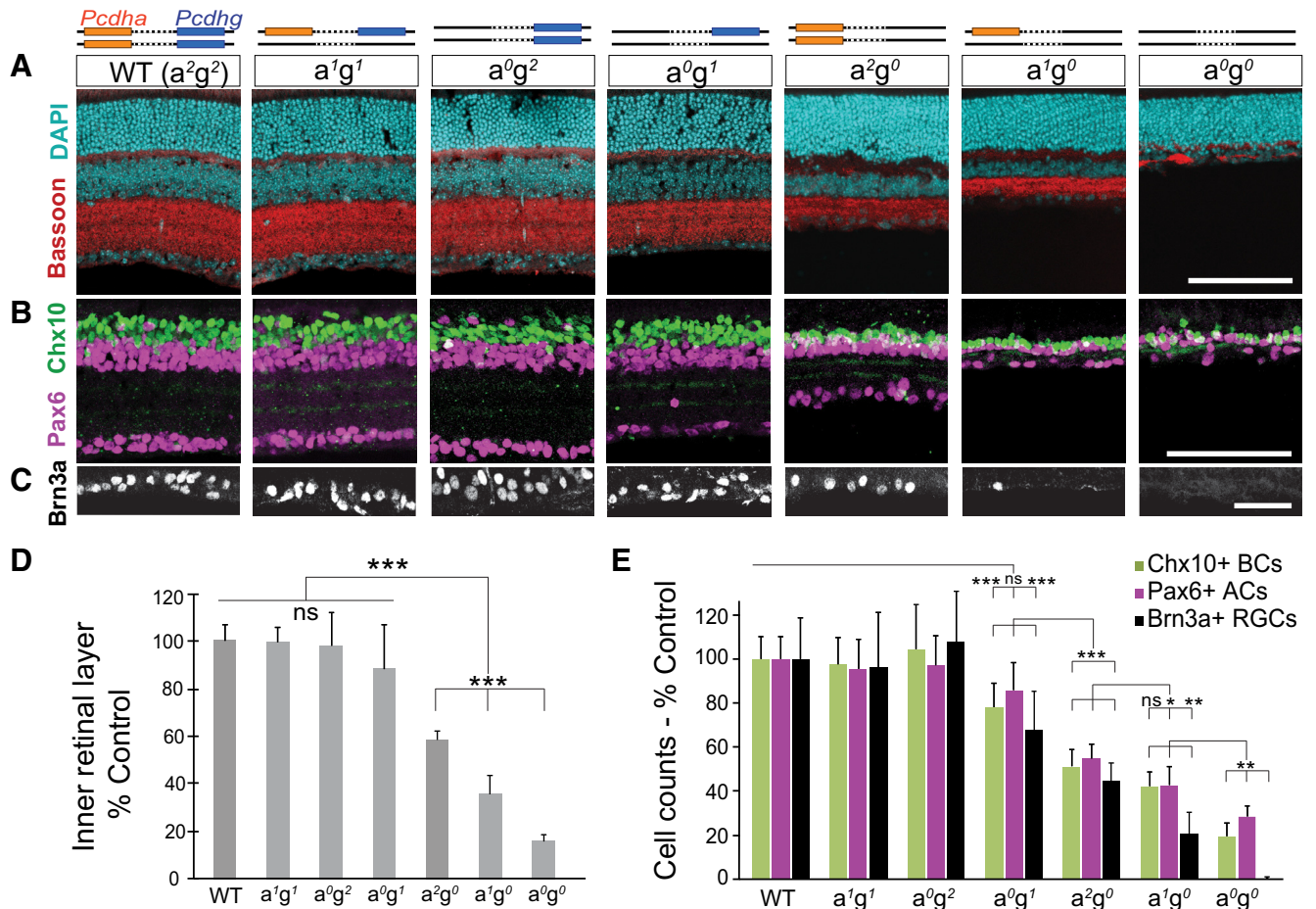


**Figure 6.** Dose-dependent effects of *Pcdha* and *Pcdhg* cluster deletions on retinal survival. **A–C**, Top, schematic representation of serial *Pcdha* (*a*, orange) and *Pcdhg* (*g*, blue) cluster deletions in seven *Pcdh* genotypes.  $a^xg^y$  are used to abbreviate the genotypes, where *x* denotes the number of WT alleles. Successive cluster deletions result in progressive decreases in inner retina layer thickness and cell number. **A**, Retina sections stained with DAPI (cyan) and anti-Bassoon (red). **B**, **C**, Interneurons and RGCs immunostained for Chx10+ BCs (green), Pax6+ ACs (magenta), and Brn3a+ RGCs (white). **D**, Quantifications of inner retina thickness (sum of the INL, IPL, and GCL). One-way ANOVA  $F_{(8,132)} = 182.3, p < 0.0001, n = 20$  sections, 3–4 animals per genotype. **E**, Interneuron and RGC cell counts. Chx10+: one-way ANOVA  $F_{(9,185)} = 99.2, p < 0.0001$ ; Pax6: one-way ANOVA  $F_{(9,185)} = 96.9, p < 0.0001$ ; Brn3a+: one-way ANOVA  $F_{(9,143)} = 64.5, p < 0.0001$ . Bars show means normalized as percentage control sibling data with percentage SD.  $n = 15$  or 17 images, 4–5 animals per genotype. \*\*\* $p < 0.001$ , \*\* $p < 0.01$ , \* $p < 0.05$ , pairwise Tukey tests. Scale bars: A, B, 100  $\mu\text{m}$ ; C, 50  $\mu\text{m}$ .

sate for the loss of one copy of the *Pcdhg* cluster (*Pcdh-a*<sup>1</sup>*g*<sup>1</sup>), providing the minimum threshold of survival activity required for WT levels of interneurons and RGCs. Further comparisons confirmed that the *Pcdha* cluster partially compensates for the absence of *Pcdhgs* in a dose-dependent manner, as shown by the graded effect of *Pcdha* cluster copy on enhancing inner retina thickness and cell number (*Pcdh-a*<sup>2</sup>*g*<sup>0</sup>, *Pcdh-a*<sup>1</sup>*g*<sup>0</sup>, *Pcdh-a*<sup>0</sup>*g*<sup>0</sup>).

We also examined *Pcdh-ag*<sup>ff</sup> (*Pcdh-a*<sup>0</sup>*g*<sup>ff</sup>) retinas, in which the targeted *Pcdhg*<sup>f</sup> locus remains intact but is hypomorphic. Inner retinal phenotypes trended between those of *Pcdh-a*<sup>0</sup>*g*<sup>1</sup> and *Pcdh-a*<sup>2</sup>*g*<sup>0</sup> retinas. Numbers of bipolar cells and RGCs in *Pcdh-a*<sup>0</sup>*g*<sup>ff</sup> retinas did not differ from those in *Pcdh-a*<sup>0</sup>*g*<sup>1</sup> retinas, but were significantly greater compared to *Pcdh-a*<sup>2</sup>*g*<sup>0</sup> retinas (Chx10+ BCs: one-way ANOVA,  $F_{(3,72)} = 67.3, p < 0.0001$ ; *Pcdh-a*<sup>0</sup>*g*<sup>ff</sup>, 85% control; *Pcdh-a*<sup>0</sup>*g*<sup>1</sup>, 78%,  $p = 0.18$  *post hoc* Tukey test for  $a^2g^{ff} - a^0g^1$ ; *Pcdh-a*<sup>2</sup>*g*<sup>0</sup>, 51% control,  $p = 0.001$ , Tukey test for  $a^0g^{ff} - a^2g^0$ ; Brn3a+ RGCs: one-way ANOVA  $F_{(3,62)} = 21.7, p < 0.0001$ ; *Pcdh-a*<sup>2</sup>*g*<sup>ff</sup>, 62%; *Pcdh-a*<sup>0</sup>*g*<sup>1</sup>, 68%,  $p = 0.80$ , Tukey test; *Pcdh-a*<sup>2</sup>*g*<sup>0</sup>, 45% control,  $p = 0.048$ , Tukey test). The inner retinal layers in *Pcdh-a*<sup>0</sup>*g*<sup>ff</sup> retinas were intermediate in thickness between those of *Pcdh-a*<sup>0</sup>*g*<sup>1</sup> and *Pcdh-a*<sup>2</sup>*g*<sup>0</sup> retinas (*Pcdh-a*<sup>0</sup>*g*<sup>ff</sup>, 70% control; *Pcdh-a*<sup>0</sup>*g*<sup>1</sup>, 81%,  $p = 0.0053$  Tukey

test; *Pcdh-a*<sup>2</sup>*g*<sup>0</sup>, 58% control,  $p = 0.001$  *post hoc* Tukey test. One-way ANOVA  $F_{(3,72)} = 52.2, p < 0.0001$ ). Therefore, the homozygous *Pcdh-ag*<sup>f</sup> allele is approximately functionally equivalent to a heterozygous *Pcdhg*-null allele.

Together, these data show that, despite the absence of a detectable loss of cells in *Pcdha* mutant retinas, the *Pcdhas* cooperate with the *Pcdhgs* in a dose-dependent fashion to support the survival of retinal interneurons and RGCs.

#### **Pcdhas and Pcdhgs cooperate to mediate dendritic self-avoidance**

The radial and uniform distribution of SAC dendrites arises from a process of self-avoidance, whereby sibling dendritic branches repel each other, leading to even coverage of their territory. We showed that *Pcdhgs* are critical mediators of dendritic self-avoidance in SACs (Lefebvre et al., 2012). *Pcdhas* are also expressed by SACs (Fig. 1D) and *Pcdhbs* are broadly expressed in the INL and GCL, suggesting that they may also be involved in SAC dendrite self-avoidance. To test this possibility, we first compared SAC morphology in *Pcdha*<sup>ko</sup>, *Pcdhb*<sup>ko</sup>, and *Pcdhg*<sup>rko</sup> mutants by sparse labeling with a recombinant AAV expressing a membrane-tagged red fluorescent protein. As reported previously, dendrites

of single SACs frequently crossed each other and formed loose bundles in *Pcdhg*<sup>rk0</sup> mutants (Fig. 7A). In contrast, the morphology of SACs in *Pcdha*<sup>ko</sup> and *Pcdhb*<sup>ko</sup> retinas were indistinguishable from that in controls (Fig. 7A).

To assess interactions between Pcdhas and Pcdhgs in SAC dendritic arborization, we initially examined *Pcdh-ag*<sup>rk0</sup> mutants. Although the number of amacrine cells was reduced by ~72% in *Pcdh-ag*<sup>rk0</sup> (Fig. 6E), the number of SACs was reduced by only ~10% (Fig. 7B; unpaired *t* test,  $t_{(32)} = 2.0$ ,  $p = 0.059$ ;  $n = 17$  regions of interest, 3 animals per genotype), consistent with results from *Pcdhg*<sup>rk0</sup> mutants (~45% loss of all amacrine (Fig. 6E), but there was no detectable loss of SACs (Lefebvre et al., 2012)). Nonetheless, we were concerned that interpretation of defects in SAC morphology would be confounded by the loss of their synaptic partners and by the collapse of the two SAC strata (Fig. 7C). To circumvent this problem, we deleted *Pcdhgs* selectively from SACs using a ChAT-cre line (*Pcdh-ag*<sup>fl/fl</sup>;ChAT<sup>cre</sup> or *Pcdh-ag*<sup>SACko</sup>). Compared with *Pcdh-ag*<sup>rk0</sup> retinas, the stratification of SAC processes was preserved in *Pcdh-ag*<sup>SACko</sup> retinas, although some gaps were present (Fig. 7C). The inner retina was also preserved in *Pcdh-ag*<sup>SACko</sup> because inner retina layer thickness and numbers of RGCs were indistinguishable from control *Pcdh-ag*<sup>fl/fl</sup> retinas (INL-GCL layers: *Pcdh-ag*<sup>SACko</sup>,  $73.5 \pm 1.8$   $\mu\text{m}$ ; *Pcdh-ag*<sup>fl/fl</sup>,  $70.7 \pm 2.2$   $\mu\text{m}$ ;  $n = 12$  sections from 3–4 animals; unpaired *t* test,  $t_{(22)} = 0.98$ ,  $p = 0.34$ . Brn3a+ RGCs: *Pcdh-ag*<sup>SACko</sup>,  $14.8$  cells/area  $\pm 0.8$ ; *Pcdh-ag*<sup>fl/fl</sup>,  $15.7$  cells/area  $\pm 1.1$ ;  $n = 15$  sections from 3–4 animals; unpaired *t* test,  $t_{(28)} = 0.68$ ,  $p = 0.50$ ). Moreover, terminals of amacrine and bipolar subtypes segregated to appropriate IPL sublaminae (Fig. 7D), similar to WT (see Fig. 5A, C). Therefore, deletion of *Pcdhgs* in SACs in a *Pcdh-a*<sup>ko</sup>-null background had no detectable non-cell-autonomous effects.

When viewed in whole mount, the SAC dendritic plexus was clearly disorganized in *Pcdh-ag*<sup>SACko</sup> retinas. Defects were more severe in this genotype than in single *Pcdhg*<sup>rk0</sup> and *Pcdhg*<sup>SACko</sup> mutants. *Pcdha*<sup>ko</sup> mutant retinas were unaffected. Conversely, SAC dendrites were more dramatically disorganized in double *Pcdh-ag*<sup>rk0</sup> retinas than in *Pcdh-ag*<sup>SACko</sup> mutants (Fig. 7E, F). Given the absence of non-cell-autonomous effects in *Pcdh-ag*<sup>SACko</sup> retinas, we conclude that the more striking defects in *Pcdh-ag*<sup>rk0</sup> SACs result from non-cell-autonomous effects and therefore used *Pcdh-ag*<sup>SACko</sup> for further studies of SAC morphology.

Individually labeled *Pcdh-ag*<sup>SACko</sup> SACs displayed dendrite crossing and bundling defects that were dramatically more pronounced than those in *Pcdhg* mutants. The dendrites formed larger fascicles and, in the majority of cases, they lost radial symmetry (Fig. 7G). The collapse was so severe that it was infeasible to count individual branches or crossings as we had done for *Pcdhg* mutants (Lefebvre et al., 2012). We therefore devised an alternative method to quantify the difference between *Pcdhg*<sup>SACko</sup> and *Pcdh-ag*<sup>SACko</sup> SACs by measuring radial symmetry. Examples are shown in Figure 8, A and B. Whereas the radial symmetry of SAC arbors was degraded to a small but significant extent in *Pcdhg*<sup>SACko</sup> retinas, it was nearly abolished in *Pcdh-ag*<sup>SACko</sup> retinas (Fig. 8C; one-way ANOVA,  $F_{(3,64)} = 42.1$ ,  $p < 0.0001$ , Tukey's test,  $p < 0.0001$ , except for WT- $a^2g^0$ ,  $p = 0.042$ ;  $n = 17$  SACs, 2–4 animals from genotype). Moreover, the radius of the SAC arbor did not differ significantly between WT and *Pcdhg*<sup>SACko</sup> retinas, but was significantly decreased in *Pcdh-ag*<sup>SACko</sup> (Fig. 8D; one-way ANOVA,  $F_{(3,64)} = 13.4$ ,  $p < 0.0001$ ; Tukey's test,  $p < 0.0001$ , except for WT- $a^2g^0$ ,  $p = 0.80$ ). We also analyzed SACs from *Pcdhg*; *Pcdh-ag*<sup>SACko</sup> transheterozygous mice, which retained one copy of the *Pcdha* cluster ( $a^1g^0$ ). SAC defects were intermediate in severity between those of *Pcdhg* and *Pcdh-ag* mutants (Fig. 8A–D), reveal-

ing the dose-dependent contributions of Pcdhas. Therefore, Pcdhas and Pcdhgs cooperate to mediate dendritic self-avoidance.

### Pcdhas and Pcdhgs make equal contributions to dendrite self-avoidance in Purkinje cells

Pcdhgs are required for dendritic self-avoidance in cerebellar Purkinje cells and in SACs (Lefebvre et al., 2012). Because Purkinje cells stochastically express subsets of both *Pcdha* and *Pcdhg* isoforms (Esumi et al., 2005; Kaneko et al., 2006), we investigated whether Pcdhas affect the patterning of Purkinje cells dendrites either alone or in combination with Pcdhgs. We labeled individual Purkinje cells in *Pcdha*<sup>ko</sup> and WT animals by injection of AAV encoding GFP into neonatal mice. Deletion of the Pcdhas led to self-avoidance defects, including branch overlaps and overall disorganization of branching (Fig. 9A, B). Self-crossing dendrites were distinguished by branch intersections detected in single confocal planes and close apposition of branches in orthogonal views (Fig. 9A', B'). The severity and rate of self-crossing defects in *Pcdh-a*<sup>ko</sup> mutants were similar to those in *Pcdh-g*<sup>PCKo</sup> mutants (*PCKo*: with Purkinje-specific Cre driver, *Pcp2-cre*) (Fig. 9C, C') (Lefebvre et al., 2012). Therefore, in contrast to SACs, in which Pcdhas have no discernable effect on their own, the *Pcdha* and *Pcdhg* clusters have similar functions in dendrite self-avoidance of Purkinje cells.

Finally, we deleted both *Pcdhas* and *Pcdhgs* from Purkinje cells by injecting AAV vectors encoding Cre and a Cre-dependent fluorescent reporter into perinatal *Pcdh-ag*<sup>fl/fl</sup> mutants (*Pcdh-ag*<sup>PCKo</sup>). In the absence of both clusters, Purkinje cells developed a dramatic excess of dendritic branches and a greater frequency of branch self-overlaps (570%, normalized as percentage of branch overlaps in control littermates) compared with single *Pcdh-a*<sup>ko</sup> (252%,  $p < 0.0001$ , Mann–Whitney test) or *Pcdh-g*<sup>PCKo</sup> Purkinje cells (245%,  $p < 0.0001$ , Mann–Whitney test; Fig. 9D, D', E). Although we cannot exclude non-cell-autonomous effects of constitutive *Pcdha* deletions in *Pcdha*<sup>ko</sup> and *Pcdh-ag* mutant cerebellums, double *Pcdh-ag*<sup>PCKo</sup> Purkinje cells were generated by sparse deletion of *Pcdhg* and these cells revealed a significant interaction between Pcdhas and Pcdhgs in dendritic defects. We noted that arbor area was significantly reduced in double mutant Purkinje cells ( $p = 0.002$ , Mann–Whitney test), whereas those of single mutant Purkinje cells were unaffected (*Pcdh-a*<sup>ko</sup>,  $p = 0.37$  and *Pcdh-g*<sup>PCKo</sup>,  $p = 0.89$ , Mann–Whitney test; Fig. 9F). In contrast, when viewed along the  $y$ - $z$  axis (parasagittal plane), the arbors of *Pcdh-ag*<sup>PCKo</sup> cells occupied increased space compared with control, with multiple sets of overlapping of dendrites spanning the entire arbor (Fig. 9G, H). The multiplanar arrangement of *Pcdh-ag*<sup>PCKo</sup> Purkinje dendrites differed qualitatively from the monopolar arbor formed by control Purkinje cells (Fig. 9I, J; Kaneko et al., 2011). Therefore, deletion of both *Pcdha* and *Pcdhg* clusters affects multiple aspects of Purkinje arbor organization, including area and monopolarity.

Together, these findings reveal that the Pcdhas and Pcdhgs serve equal roles in Purkinje cells and that Pcdh diversity provided by both clusters is essential for optimal dendrite patterning. Importantly, they also show that the Pcdhas are not generally subordinate in effect to Pcdhgs, but differ in their contributions in a cell-type-specific manner. The dose-dependent and cell-type-specific contributions of Pcdhas and Pcdhgs in retinal survival and SAC and Purkinje dendrite self-avoidance are summarized in Table 1.

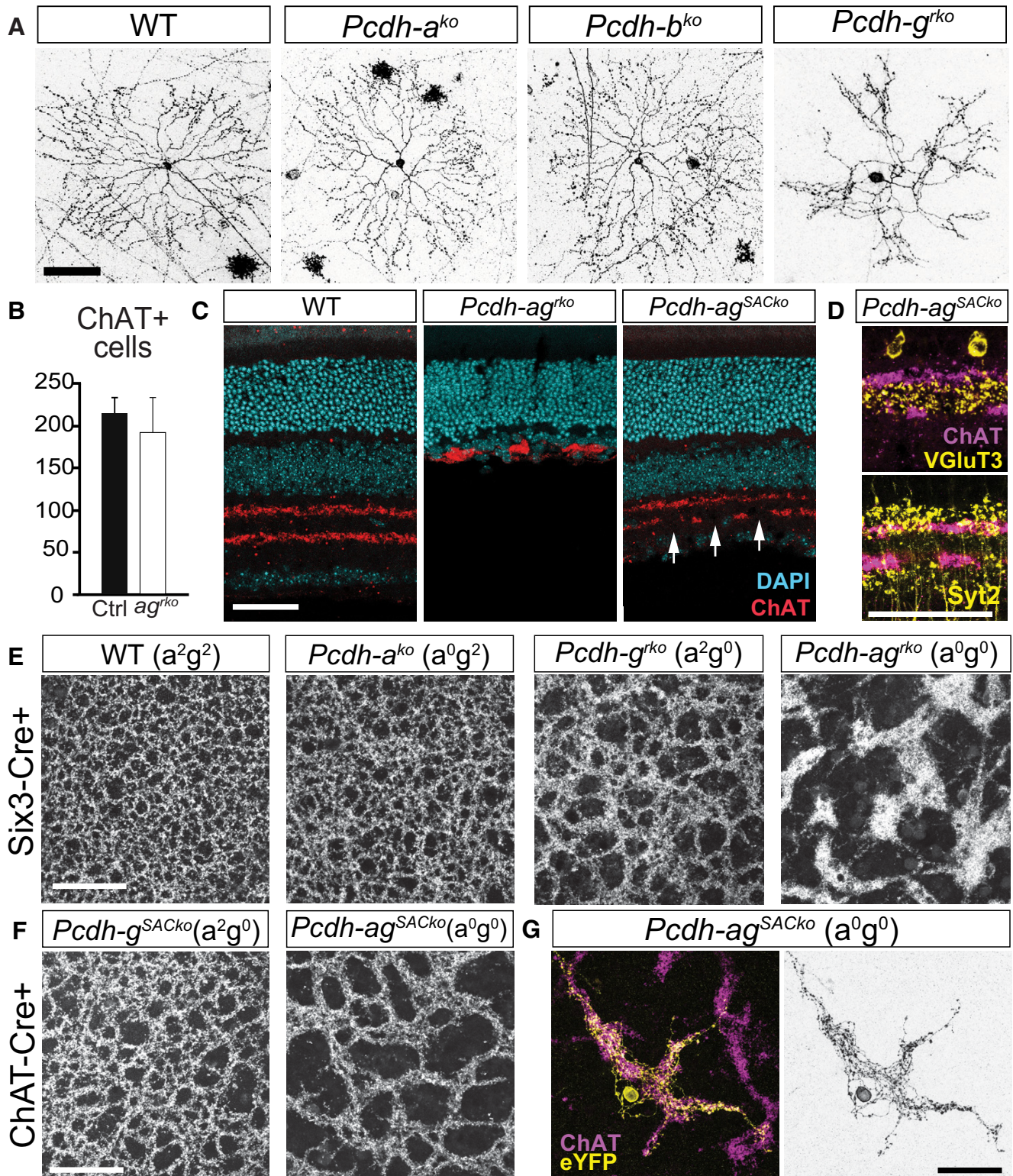


**Figure 7.** The *Pcdha* and *Pcdhg* clusters cooperate to promote dendrite self-avoidance. **A**, Single SACs labeled with AAV-membrane-RFP in WT, *Pcdh-a<sup>ko</sup>*, *Pcdh-b<sup>ko</sup>*, and *Pcdh-g<sup>rko</sup>* retinal whole mounts. **B**, Numbers of ChAT+ SACs in WT and *Pcdh-ag<sup>rko</sup>* retinas. Bars show means  $\pm$  SEM.  $n = 17$  areas were analyzed, 3 animals per genotype, Student's *t* test,  $t_{(32)} = 2.0$ ,  $p = 0.059$ . **C**, SAC dendritic layers in WT, *Pcdh-ag<sup>rko</sup>*, and *Pcdh-ag<sup>SACko</sup>* [*Pcdh-a<sup>conexidell</sup>; g<sup>f</sup> x Chat-cre*] retinas labeled with DAPI (cyan) and anti-ChAT (red). Arrows indicate gaps in the SAC layers despite preservation of the inner retina in *Pcdh-ag<sup>SACko</sup>* retina. **D**, Laminar segregation of vGluT3+ AC processes (yellow, top) and Syt2+ BC terminals (yellow, bottom) is intact in *Pcdh-ag<sup>SACko</sup>* retina (ChAT+ SAC layers, magenta). **E, F**, Whole-mount retina preparation showing ChAT-labeled plexus formed by SAC dendrites in WT, single *Pcdh-a<sup>ko</sup>* and *Pcdh-g<sup>rko</sup>* mutants, and double *Pcdh-ag<sup>rko</sup>* mutants (**E**) and SAC-specific *Pcdh-g<sup>SACko</sup>* and *Pcdh-ag<sup>SACko</sup>* mutants (**F**). Note larger gaps and increased fasciculation of SAC plexus in double mutant *Pcdh-ag* compared with WT or single *Pcdhg* mutant retinas. **G**, Morphology of a single SAC from *Pcdh-ag<sup>SACko</sup>* retina labeled with eYFP (yellow) and SAC plexus labeled with anti-ChAT (magenta). Scale bars, 50  $\mu$ m.

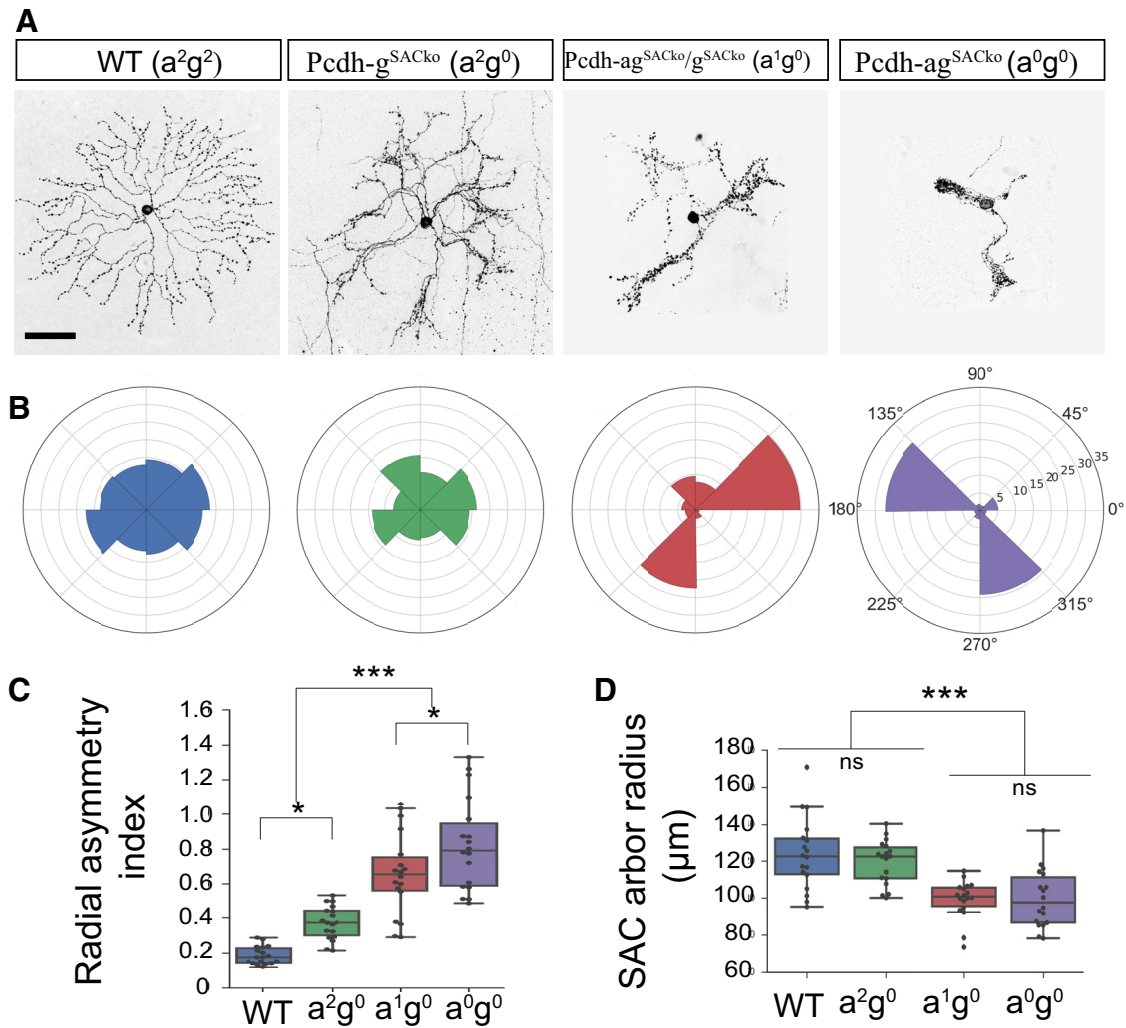


**Figure 8.** Dose-dependent interactions between *Pcdhas* and *Pcdhgs* clusters on SAC dendrite arborization and self-avoidance. **A**, Morphology of single SACs reveal effects of removing a single ( $a^1g^0$ ) or both *Pcdha* clusters ( $a^0g^0$ ) on dendrite self-avoidance in SACs lacking *Pcdhgs* ( $Pcdh-g^{SACko}$ ). **B**, Polar plot representations for SACs in **A** showing the pixel distribution of dendrites across eight polar segments. **C**, Analysis of SAC polar plots such as those in **B** using an asymmetry index, which reports on the SDs from expected radial symmetry (index 0.0) in which pixels are equally distributed. One-way ANOVA,  $F_{(3,64)} = 42.1, p < 0.0001$ . Tukey's multiple-comparisons tests,  $p < 0.0001$ , with the exception of pairs WT- $a^2g^0$ ,  $p = 0.018$ , and  $a^1g^0$ - $a^0g^0$ ,  $p = 0.042$ . **D**, Box plots showing SAC dendritic field radius. One-way ANOVA,  $F_{(3,64)} = 13.4, p < 0.0001$ . Tukey's multiple-comparisons tests,  $p < 0.0001$ . Pairs WT- $a^2g^0$ ,  $p = 0.80$ , and  $a^1g^0$ - $a^0g^0$ ,  $p = 0.90$  are not significant (ns). **C, D**,  $n = 17$  SACs, 2–4 animals from genotype. \*\*\* $p < 0.0001$ , \* $p < 0.05$ . Scale bars, 50  $\mu\text{m}$ .

## Discussion

The clustered *Pcdhs* have the potential to generate extraordinary cell surface diversity and specificity for patterning the nervous system. They do so by combinatorial interactions among *Pcdh* members: each *Pcdh* exhibits homophilic binding in *trans*, but multimerizes promiscuously in *cis*. Selective *trans* binding between matching combinations can then greatly expand the recognition specificity presented by *Pcdh* multimers (Schreiner and Weiner, 2010; Thu et al., 2014; Nicoludis et al., 2015; Rubinstein et al., 2015; Goodman et al., 2016; Rubinstein et al., 2017). Here, we demonstrate that the *Pcdhas* and *Pcdhgs* interact to promote neuronal survival in retina and dendritic self-avoidance in both retina and cerebellum. However, interactions between the clusters differ between these tissues (Table 1). In retina, loss of *Pcdhas* has no obvious consequence, but defects in *Pcdha/Pcdhg* double mutants are dramatically more severe than those of *Pcdhg* mutants. In contrast, defects in dendritic patterning of cerebellar Purkinje cells are significant in both *Pcdha* and *Pcdhg* mutants and markedly more severe in *Pcdha/Pcdhg* double mutants. These

patterns have been called unequal and partial redundancy, respectively (Briggs et al., 2006; Barbaric et al., 2007).

### Unequal redundancy of *Pcdhas* and *Pcdhgs* in retinal development

Duplicated genes can play redundant, overlapping, or completely distinct roles. For the *Pcdh* clusters, there are at least three factors relevant to their relationships. First, the selective homophilic specificity of *Pcdh trans* interactions implies that *Pcdha* and *Pcdhg* proteins can mediate different intercellular interactions. Second, *Pcdhas* and *Pcdhgs* have different intracellular domains and could therefore engage distinct signaling pathways. Third, expression patterns of *Pcdha* and *Pcdhg* genes differ because of distinct regulatory elements (Ribich et al., 2006; Noguchi et al., 2009; Kehayova et al., 2011; Yokota et al., 2011). Determining the extent of redundancy among *Pcdh* clusters has been challenging due to the complexity of the locus and the presence of essential genes. Recent studies of double and triple *Pcdh* cluster mutants from two groups have revealed redundant and cooperative func-

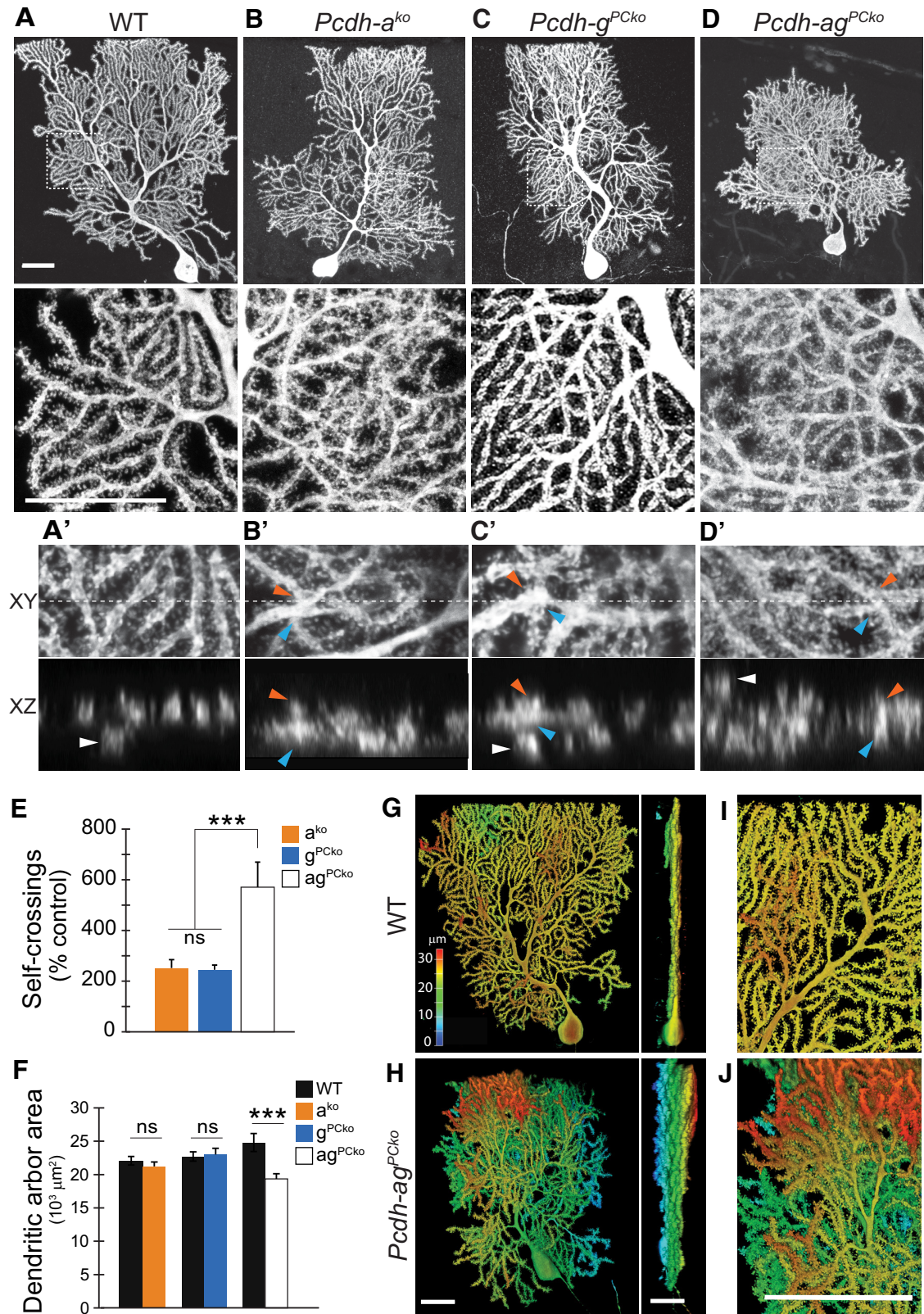


**Figure 9.** *Pcdhas* are essential for dendrite self-avoidance of Purkinje cells and serve equal functions with *Pcdhgs*. **A–D**, Morphology of single mature (P35) cerebellar Purkinje cells labeled with AAV-GFP or AAV-RFP. Areas boxed in top panels are shown at higher magnification in bottom. Purkinje cells lacking *Pcdha*, *Pcdhg*, or both clusters display disorganized arborizations marked by frequent self-crossing defects, but defects are more dramatic in double than single mutants. Double mutant Purkinje cells also exhibit increased branching and smaller dendritic territories. **A'–D'**, Orthogonal *x–y* (top) and *x–z* (bottom) views of dendrite self-crossings in high-magnification confocal stacks. Blue and orange arrowheads mark intersecting branches in the *x–y* plane (maximum projection of substack; dashed line is plane for *x–z* sectioning) and their close apposition in *x–z* (note merged fluorescent signals from two branches). “Overpassing” branches that extend in distant planes are individually resolved in *x–z* (white arrowheads) and are not counted as self-crossings. Single and double *Pcdh* mutant Purkinje cells display increased self-crossings and overpassing branches compared with WT. **E**, Quantifications of dendrite self-crossings detected in 70 × 70 μm areas from z-stack confocal images. Bars show (Figure legend continues.)

**Table 1. Summary of *Pcdh* cluster dosage relationships in retina and Purkinje cell development**

Pcdh clusters	Genotype	Inner retina cell survival	SAC dendrite self-avoidance	Purkinje dendrite self-avoidance
Pcdh a <sup>2</sup> g <sup>2</sup>	<i>Pcdh-a</i> <sup>wt;g<sup>wt</sup></sup>	–	–	–
a <sup>1</sup> g <sup>1</sup>	<i>Pcdh-ag</i> <sup>+ /cko</sup> ( <i>rko</i> , <i>Six3-cre</i> ; <i>PCKo</i> , <i>Pcp2-cre</i> )	–	–	–
a <sup>0</sup> g <sup>2</sup>	<i>Pcdh-a</i> <sup>ko /ko</sup>	–	–	×
a <sup>0</sup> g <sup>1</sup>	<i>Pcdh-a</i> <sup>ko /-ag<sup>cko</sup></sup>	×	nd	nd
a <sup>2</sup> g <sup>0</sup>	<i>Pcdh-g</i> <sup>cko /cko</sup>	×	×	×
a <sup>1</sup> g <sup>0</sup>	<i>Pcdh-ag</i> <sup>cko /-g<sup>cko</sup></sup>	×	×	nd
a <sup>0</sup> g <sup>0</sup>	<i>Pcdh-ag</i> <sup>cko /cko</sup>	×	×	×
SAC-specific a <sup>2</sup> g <sup>0</sup>	<i>Pcdh-g</i> <sup>SACKo /ko</sup> ( <i>Chat-Cre</i> )	–	×	–
SAC - a <sup>1</sup> g <sup>0</sup>	<i>Pcdh-ag</i> <sup>SACKo /-g<sup>SACKo</sup></sup>	–	×	–
SAC - a <sup>0</sup> g <sup>0</sup>	<i>Pcdh-ag</i> <sup>SACKo /SACKo</sup>	–	×	–

Phenotype score: –, unaffected; ×, disrupted and graded by severity (×n); nd, not determined.

tions in multiple aspects of embryonic CNS development (Hasegawa et al., 2016; Mountoufaris et al., 2017). To study Pcdh cluster diversity in the postnatal CNS, we generated a double *Pcdha*;*Pcdhg* mutant allele in which *Pcdhg* could be inactivated conditionally, preserving postnatal viability. By comparing *Pcdh* cluster expression and mutant retinas lacking one or both clusters, we discovered both overlapping and distinct features of Pcdhas and Pcdhgs in retinal development. Our principal results are as follows.

First, although *Pcdhas* and *Pcdhgs* (as well as *Pcdhbs*) are broadly expressed in the inner retina, removal of the *Pcdhgs* led to loss of RGCs, bipolar cells, and amacrine cells (Lefebvre et al., 2008), whereas removal of *Pcdhas* had no detectable effect on their survival. In contrast, removal of both *Pcdha* and *Pcdhg* clusters enhanced the *Pcdhg* phenotype, unmasking shared roles for the Pcdhas in survival of inner retinal cells.

Second, *Pcdhas* expression is strikingly higher in RGCs than in other retinal cells and survival of RGCs is more dramatically affected than survival of bipolar or amacrine cells in *Pcdh-ag* mutants. These patterns suggest a unique role of Pcdhas in RGC development, but the nature of this role is unclear. Pcdhas are required for organizing RGC axons in the lateral geniculate nucleus (Meguro et al., 2015). Roles of Pcdhgs in this process remained to be determined, but it is intriguing to speculate that the devastating loss of RGCs in *Pcdha*/*Pcdhg* double mutants might result in part from loss of target-derived support consequent to target defects in double mutants.

Third, Pcdhas and Pcdhgs show unequally redundant roles of the morphogenesis of SAC dendrites. In *Pcdhg* mutants, dendritic

branches fail to repel each other, a phenomenon called self-avoidance, resulting in loss of the radially symmetrical morphology (Lefebvre et al., 2012). We detected no self-avoidance defects in *Pcdha* mutants, but found a striking exacerbation of the *Pcdhg* phenotype in double mutants. Our previous analysis demonstrated that restoration of a single *Pcdhg* is sufficient to rescue self-avoidance in *Pcdhg* cluster mutants, but that expression of multiple *Pcdhgs* is required for self-/non-self-discrimination in which SAC dendrites can synapse on dendrites of other SACs while avoiding sibling dendrites (Lefebvre et al., 2012; Kostadinov and Sanes, 2015). Analysis of self-/non-self-discrimination in *Pcdha*/*Pcdhg* double mutants is a promising means of probing the relationship of redundancy between entire clusters to redundancy among isoforms.

Fourth, Pcdhas partially compensate for loss of Pcdhgs in a dose-dependent manner, revealing interactions between Pcdhas and Pcdhgs in retinal survival and SAC dendrite self-avoidance. Similarly in spinal cord, redundant but unequal roles were demonstrated for the *Pcdha* and *Pcdhb* clusters in survival (Hasegawa et al., 2016). Increased apoptosis was also noted in embryonic retinas from triple *Pcdh-abg*<sup>ko</sup> (Hasegawa et al., 2016), but analysis was limited due to the immaturity of retinal cell types at this stage.

Fifth, threshold levels of Pcdh activity are required for survival and self-avoidance. In the absence of *Pcdhas*, a single *Pcdhg* cluster was haploinsufficient for survival, but addition of a *Pcdha* cluster restored cell number to WT levels. Together with dose-dependent contributions of Pcdhas, these data demonstrate that the Pcdhas signal with Pcdhgs to promote survival. By extension, we surmise that subthreshold levels of Pcdh activity in brainstem and spinal circuits contributes to the neonatal lethality frequently encountered among *Pcdh-ag*<sup>f</sup> mutants.

Divergent *Pcdha* and *Pcdhg* activities could arise from differences in expression or in biochemical or signaling properties associated with their distinct cytoplasmic regions. Our finding that the Pcdhas only partially compensate for RGC survival despite high expression levels suggests that differences in expression levels are unlikely to account for differences in survival. Given the crucial roles for the three C-type Pcdhgs isoforms in survival (Chen et al., 2012), the *Pcdha*-dependent contributions to survival could be mediated by the two C-type Pcdhas, which are more closely related to the C-type Pcdhgs than to the alternate Pcdhas.

### Partial redundancy of Pcdhas and Pcdhgs in cerebellar Purkinje cells

In contrast to SACs, Purkinje neurons are equally dependent on the Pcdhas and Pcdhgs for dendrite self-avoidance. Removal of either Pcdh cluster results in modest but clear phenotypes, whereas dual inactivation of the clusters dramatically enhanced Purkinje dendrite arborization defects. These findings reflect a partial redundancy for Pcdhas and the Pcdhgs. Therefore, the Pcdhas are not necessarily the weaker paralogs and Pcdh cluster diversity is essential for neuronal patterning of some cell types. Moreover, our results indicate that functional interactions between Pcdh clusters will differ among cell types or contexts.

Interestingly, the dendritic phenotypes in double *Pcdh* mutant SAC and Purkinje cells were qualitatively different. *Pcdh-ag* mutant Purkinje cells were multiplanar with an excess of branches. This phenotype might arise from retraction defects, which is consistent with live-imaging studies showing retraction of Purkinje dendrites upon contact with sibling (self) branches (Fujishima et al., 2012). Fujishima et al. (2012) also showed that self-contacts

←

(Figure legend continued.) means ± SEM normalized as percentage of quantifications from control siblings; n = 10–15 cells, two-way ANOVA, \*\*\*p < 0.001. **F**, Area of dendritic arborizations. Bars show mean ± SEM. n = 15–17 cells per genotype. Purkinje arbor area in *Pcdha*<sup>ko</sup> and *Pcdhg*<sup>PCKo</sup> are not significantly different from control (p = 0.37 and p = 0.89). *Pcdh-ag*<sup>PCKo</sup> arbors are significantly reduced in size compared with littermate controls (p = 0.003, Mann–Whitney U test) and when compared with the combined pool of controls (\*\*\*p = 0.0004, Mann–Whitney U test). Data on *Pcdhg* mutants in **E** and **F** are from Lefebvre et al. (2012). **G**, **H**, Depth representation of WT and *Pcdh-ag*<sup>PCKo</sup> Purkinje arborization with color spectrum code depicting positions in z (sagittal planes). Left, x–y view of depth-coded 3D rendering of Purkinje cells. Right, y–z rotation (parasagittal planes). Arbors of WT Purkinje cells are confined to narrow sagittal planes. Dendrites of *Pcdh-ag*<sup>PCKo</sup> Purkinje cells arborize into multiple planes spanning nearly the entire depth-spectrum. **I**, **J**, High-magnification view of monoplanar arrangement of WT dendritic arbors and multiplanarity of *Pcdh-ag*<sup>PCKo</sup> arbors. Note light blue branches beneath the red-colored dendrites (white arrow). Scale bars, 25 μm.

and retractions occur at terminal branch tips, which is also the site of branch addition. Pcdhs might therefore couple dendrite self-recognition with elimination in Purkinje cells to limit branch number and overlap. Whereas dendrite–dendrite interactions within a cell (self-avoidance) are degraded in single *Pcdh* mutants, dendrite–dendrite interactions between cells (termed tiling) may also be comprised in double mutants. Conversely, *Pcdh-ag* mutant SACs displayed increased fasciculation between sibling dendrites, which severely distorted the radial organization. SAC dendrites tend to cofasciculate (Lefebvre et al., 2012), which is critical for establishing reciprocal connections with neighboring SACs, but it must be minimized among sibling dendrites (Kostadinov and Sanes, 2015). Although further analyses are required to determine the underlying mechanisms, our observations raise the possibility that Pcdhs mediate self-avoidance in mammalian neurons through diverse cellular processes such as branch elimination and repulsion.

### Overlapping but distinct roles for Pcdhs in neuronal development

Two recent studies have demonstrated cooperation among Pcdh clusters in the embryonic olfactory system. Olfactory sensory neurons (OSNs) terminate onto shared glomeruli in the olfactory bulb. In triple *Pcdh-abg*<sup>ko</sup> mutant neonates, OSN reached their target but collapsed and failed to elaborate branches (Mountoufaris et al., 2017). Glomerular defects were more severe in triple *Pcdh-abg*<sup>ko</sup> neonates than in single cluster mutants (Hasegawa et al., 2016; Mountoufaris et al., 2017). Our results extend this analysis to postnatal development and demonstrate interactions between clusters in two other regions: retina and cerebellum. In contrast, patterning of sensory 1a afferents terminals in spinal cord are only dependent on the *Pcdhg* cluster (Prasad and Weiner, 2011; Hasegawa et al., 2016). Therefore, functional and redundant interactions between Pcdh clusters differ among cell types and developmental pathways.

Other, related studies have shown both shared and distinct roles of isoforms within the *Pcdha* and *Pcdhg* clusters (see Introduction) (Chen et al., 2012; Lefebvre et al., 2012; Kostadinov and Sanes, 2015; Chen et al., 2017). The picture emerging from these analyses is that diversity of Pcdh isoforms both within and between clusters is critically important for neural development, with both isoforms and clusters mediating overlapping yet distinct functions. With a large, functionally redundant ensemble of molecules, the clustered Pcdhs can mediate highly selective events when there are numerous potential interactions and ensure robustness during patterning of complex neuronal structures.

### References

- Barbaric I, Miller G, Dear TN (2007) Appearances can be deceiving: phenotypes of knockout mice. *Brief Funct Genomic Proteomic* 6:91–103. [CrossRef Medline](#)
- Briggs GC, Osmont KS, Shindo C, Sibout R, Hardtke CS (2006) Unequal genetic redundancies in arabidopsis—a neglected phenomenon? *Trends Plant Sci* 11:492–498. [CrossRef Medline](#)
- Cai D, Cohen KB, Luo T, Lichtman JW, Sanes JR (2013) Improved tools for the Brainbow toolbox. *Nat Methods* 10:540–547. [CrossRef Medline](#)
- Chen WV, Alvarez FJ, Lefebvre JL, Friedman B, Nwaweze C, Geiman E, Smith C, Thu CA, Tapia JC, Tasic B, Sanes JR, Maniatis T (2012) Functional significance of isoform diversification in the protocadherin  $\gamma$  gene cluster. *Neuron* 75:402–409. [CrossRef Medline](#)
- Chen WV, Nwaweze CL, Denny CA, O’Keeffe S, Rieger MA, Mountoufaris G, Kirner A, Dougherty JD, Hen R, Wu Q, Maniatis T (2017) *Pcdhalpha2* is required for axonal tiling and assembly of serotonergic circuitries in mice. *Science* 356:406–411. [CrossRef Medline](#)
- Cong L, Ran FA, Cox D, Lin S, Barretto R, Habib N, Hsu PD, Wu X, Jiang W, Marraffini LA, Zhang F (2013) Multiplex genome engineering using CRISPR/Cas systems. *Science* 339:819–823. [CrossRef Medline](#)
- Cui Q, Ren C, Sollars PJ, Pickard GE, So KF (2015) The injury resistant ability of melanopsin-expressing intrinsically photosensitive retinal ganglion cells. *Neuroscience* 284:845–853. [CrossRef Medline](#)
- Duan X, Qiao M, Bei F, Kim IJ, He Z, Sanes JR (2015) Subtype-specific regeneration of retinal ganglion cells following axotomy: effects of osteopontin and mTOR signaling. *Neuron* 85:1244–1256. [CrossRef Medline](#)
- Esumi S, Kakazu N, Taguchi Y, Hirayama T, Sasaki A, Hirabayashi T, Koide T, Kitsukawa T, Hamada S, Yagi T (2005) Monoallelic yet combinatorial expression of variable exons of the protocadherin-alpha gene cluster in single neurons. *Nat Genet* 37:171–176. [CrossRef Medline](#)
- Fujishima K, Horie R, Mochizuki A, Kengaku M (2012) Principles of branch dynamics governing shape characteristics of cerebellar Purkinje cell dendrites. *Development* 139:3442–3455. [CrossRef Medline](#)
- Furuta Y, Lagutin O, Hogan BL, Oliver GC (2000) Retina- and ventral forebrain-specific cre recombinase activity in transgenic mice. *Genesis* 26:130–132. [CrossRef Medline](#)
- Garrett AM, Weiner JA (2009) Control of CNS synapse development by  $\{\gamma\}$ -protocadherin-mediated astrocyte-neuron contact. *J Neurosci* 29:11723–11731. [CrossRef Medline](#)
- Garrett AM, Schreiner D, Lobas MA, Weiner JA (2012)  $\gamma$ -protocadherins control cortical dendrite arborization by regulating the activity of a FAK/PKC/MARCKS signaling pathway. *Neuron* 74:269–276. [CrossRef Medline](#)
- Gegonne A, Tai X, Zhang J, Wu G, Zhu J, Yoshimoto A, Hanson J, Cultraro C, Chen QR, Guinter T, Yang Z, Hathcock K, Singer A, Rodriguez-Canales J, Tessarollo L, Mackem S, Meerzaman D, Buetow K, Singer DS (2012) The general transcription factor TAF7 is essential for embryonic development but not essential for the survival or differentiation of mature T cells. *Mol Cell Biol* 32:1984–1997. [CrossRef Medline](#)
- Goodman KM, Rubinstein R, Thu CA, Bahna F, Manneppalli S, Ahlsén G, Rittenhouse C, Maniatis T, Honig B, Shapiro L (2016) Structural basis of diverse homophilic recognition by clustered alpha- and beta-protocadherins. *Neuron* 90:709–723. [CrossRef Medline](#)
- Hasegawa S, Hamada S, Kumode Y, Esumi S, Katori S, Fukuda E, Uchiyama Y, Hirabayashi T, Mombaerts P, Yagi T (2008) The protocadherin-alpha family is involved in axonal coalescence of olfactory sensory neurons into glomeruli of the olfactory bulb in mouse. *Mol Cell Neurosci* 38:66–79. [CrossRef Medline](#)
- Hasegawa S, Kumagai M, Hagihara M, Nishimaru H, Hirano K, Kaneko R, Okayama A, Hirayama T, Sanbo M, Hirabayashi M, Watanabe M, Hirabayashi T, Yagi T (2016) Distinct and cooperative functions for the protocadherin-alpha, -beta and - $\gamma$  clusters in neuronal survival and axon targeting. *Front Mol Neurosci* 9:155. [CrossRef Medline](#)
- Hasegawa S, Kobayashi H, Kumagai M, Nishimaru H, Tarusawa E, Kanda H, Sanbo M, Yoshimura Y, Hirabayashi M, Hirabayashi T, Yagi T (2017) Clustered protocadherins are required for building functional neural circuits. *Front Mol Neurosci* 10:114. [CrossRef Medline](#)
- Hirano K, Kaneko R, Izawa T, Kawaguchi M, Kitsukawa T, Yagi T (2012) Single-neuron diversity generated by protocadherin-beta cluster in mouse central and peripheral nervous systems. *Front Mol Neurosci* 5:90. [CrossRef Medline](#)
- Kaneko M, Yamaguchi K, Eiraku M, Sato M, Takata N, Kiyohara Y, Mishina M, Hirase H, Hashikawa T, Kengaku M (2011) Remodeling of monopolar purkinje cell dendrites during cerebellar circuit formation. *PLoS One* 6:e21018. [CrossRef Medline](#)
- Kaneko R, Kato H, Kawamura Y, Esumi S, Hirayama T, Hirabayashi T, Yagi T (2006) Allelic gene regulation of pcdh-alpha and pcdh-gamma clusters involving both monoallelic and biallelic expression in single purkinje cells. *J Biol Chem* 281:30551–30560. [CrossRef Medline](#)
- Katori S, Hamada S, Noguchi Y, Fukuda E, Yamamoto T, Yamamoto H, Hasegawa S, Yagi T (2009) Protocadherin-alpha family is required for serotonergic projections to appropriately innervate target brain areas. *J Neurosci* 29:9137–9147. [CrossRef Medline](#)
- Kay JN, Chu MW, Sanes JR (2012) MEGF10 and MEGF11 mediate homotypic interactions required for mosaic spacing of retinal neurons. *Nature* 483:465–469. [CrossRef Medline](#)
- Kehayova P, Monahan K, Chen W, Maniatis T (2011) Regulatory elements required for the activation and repression of the protocadherin-alpha gene cluster. *Proc Natl Acad Sci U S A* 108:17195–17200. [CrossRef Medline](#)
- Kostadinov D, Sanes JR (2015) Protocadherin-dependent dendritic self-avoidance regulates neural connectivity and circuit function. *eLife* 4.

- Lefebvre JL (2017) Neuronal territory formation by the atypical cadherins and clustered protocadherins. *Semin Cell Dev Biol* 69:111–121. [CrossRef Medline](#)
- Lefebvre JL, Zhang Y, Meister M, Wang X, Sanes JR (2008)  $\gamma$ -protocadherins regulate neuronal survival but are dispensable for circuit formation in retina. *Development* 135:4141–4151. [CrossRef Medline](#)
- Lefebvre JL, Kostadinov D, Chen WV, Maniatis T, Sanes JR (2012) Protocadherins mediate dendritic self-avoidance in the mammalian nervous system. *Nature* 488:517–521. [CrossRef Medline](#)
- Lefebvre JL, Sanes JR, Kay JN (2015) Development of dendritic form and function. *Annu Rev Cell Dev Biol* 31:741–777. [CrossRef Medline](#)
- Meguro R, Hishida R, Tsukano H, Yoshitake K, Imamura R, Tohmi M, Kitakawa T, Hirabayashi T, Yagi T, Takebayashi H, Shibuki K (2015) Impaired clustered protocadherin- $\alpha$  leads to aggregated retinogeniculate terminals and impaired visual acuity in mice. *J Neurochem* 133:66–72. [CrossRef Medline](#)
- Molmby MJ, Keeler AB, Weiner JA (2016) Homophilic protocadherin cell-cell interactions promote dendrite complexity. *Cell Rep* 15:1037–1050. [CrossRef Medline](#)
- Mountoufaris G, Chen WV, Hirabayashi Y, O’Keeffe S, Chevee M, Nwakeze CL, Polleux F, Maniatis T (2017) Multicenter pcdh diversity is required for mouse olfactory neural circuit assembly. *Science* 356:411–414. [CrossRef Medline](#)
- Nicoludis JM, Lau SY, Schärfe CP, Marks DS, Weihofen WA, Gaudet R (2015) Structure and sequence analyses of clustered protocadherins reveal antiparallel interactions that mediate homophilic specificity. *Structure* 23:2087–2098. [CrossRef Medline](#)
- Noguchi Y, Hirabayashi T, Katori S, Kawamura Y, Sanbo M, Hirabayashi M, Kiyonari H, Nakao K, Uchimura A, Yagi T (2009) Total expression and dual gene-regulatory mechanisms maintained in deletions and duplications of the pcdh cluster. *J Biol Chem* 284:32002–32014. [CrossRef Medline](#)
- Passini MA, Wolfe JH (2001) Widespread gene delivery and structure-specific patterns of expression in the brain after intraventricular injections of neonatal mice with an adeno-associated virus vector. *J Virol* 75:12382–12392. [CrossRef Medline](#)
- Pérez de Sevilla Müller L, Sargoy A, Rodriguez AR, Brecha NC (2014) Melanopsin ganglion cells are the most resistant retinal ganglion cell type to axonal injury in the rat retina. *PLoS One* 9:e93274. [CrossRef Medline](#)
- Prasad T, Weiner JA (2011) Direct and indirect regulation of spinal cord afferent terminal formation by the  $\gamma$ -protocadherins. *Front Mol Neurosci* 4:54. [CrossRef Medline](#)
- Prasad T, Wang X, Gray PA, Weiner JA (2008) A differential developmental pattern of spinal interneuron apoptosis during synaptogenesis: insights from genetic analyses of the protocadherin- $\gamma$  gene cluster. *Development* 135:4153–4164. [CrossRef Medline](#)
- Ribich S, Tasic B, Maniatis T (2006) Identification of long-range regulatory elements in the protocadherin- $\alpha$  gene cluster. *Proc Natl Acad Sci U S A* 103:19719–19724. [CrossRef Medline](#)
- Rodriguez AR, de Sevilla Müller LP, Brecha NC (2014) The RNA binding protein RBPMS is a selective marker of ganglion cells in the mammalian retina. *J Comp Neurol* 522:1411–1443. [CrossRef Medline](#)
- Rossi J, Balthasar N, Olson D, Scott M, Berglund E, Lee CE, Choi MJ, Lauzon D, Lowell BB, Elmquist JK (2011) Melanocortin-4 receptors expressed by cholinergic neurons regulate energy balance and glucose homeostasis. *Cell Metab* 13:195–204. [CrossRef Medline](#)
- Rubinstein R, Thu CA, Goodman KM, Wolcott HN, Bahna F, Manepalli S, Ahlsen G, Chevee M, Halim A, Clausen H, Maniatis T, Shapiro L, Honig B (2015) Molecular logic of neuronal self-recognition through protocadherin domain interactions. *Cell* 163:629–642. [CrossRef Medline](#)
- Rubinstein R, Goodman KM, Maniatis T, Shapiro L, Honig B (2017) Structural origins of clustered protocadherin-mediated neuronal barcoding. *Semin Cell Dev Biol* 69:140–150. [CrossRef Medline](#)
- Sanes JR, Zipursky SL (2010) Design principles of insect and vertebrate visual systems. *Neuron* 66:15–36. [CrossRef Medline](#)
- Schreiner D, Weiner JA (2010) Combinatorial homophilic interaction between  $\gamma$ -protocadherin multimers greatly expands the molecular diversity of cell adhesion. *Proc Natl Acad Sci U S A* 107:14893–14898. [CrossRef Medline](#)
- Su H, Marcheva B, Meng S, Liang FA, Kohsaka A, Kobayashi Y, Xu AW, Bass J, Wang X (2010)  $\gamma$ -protocadherins regulate the functional integrity of hypothalamic feeding circuitry in mice. *Dev Biol* 339:38–50. [CrossRef Medline](#)
- Thu CA, Chen WV, Rubinstein R, Chevee M, Wolcott HN, Felsovalyi KO, Tapia JC, Shapiro L, Honig B, Maniatis T (2014) Single-cell identity generated by combinatorial homophilic interactions between  $\alpha$ ,  $\beta$ , and  $\gamma$  protocadherins. *Cell* 158:1045–1059. [CrossRef Medline](#)
- Toyoda S, Kawaguchi M, Kobayashi T, Tarusawa E, Toyama T, Okano M, Oda M, Nakauchi H, Yoshimura Y, Sanbo M, Hirabayashi M, Hirayama T, Hirabayashi T, Yagi T (2014) Developmental epigenetic modification regulates stochastic expression of clustered protocadherin genes, generating single neuron diversity. *Neuron* 82:94–108. [CrossRef Medline](#)
- Wang X, Weiner JA, Levi S, Craig AM, Bradley A, Sanes JR (2002)  $\gamma$  protocadherins are required for survival of spinal interneurons. *Neuron* 36:843–854. [CrossRef Medline](#)
- Weiner JA, Wang X, Tapia JC, Sanes JR (2005)  $\gamma$  protocadherins are required for synaptic development in the spinal cord. *Proc Natl Acad Sci U S A* 102:8–14. [CrossRef Medline](#)
- Wu Q, Maniatis T (1999) A striking organization of a large family of human neural cadherin-like cell adhesion genes. *Cell* 97:779–790. [CrossRef Medline](#)
- Wu Q, Zhang T, Cheng JF, Kim Y, Grimwood J, Schmutz J, Dickson M, Noonan JP, Zhang MQ, Myers RM, Maniatis T (2001) Comparative DNA sequence analysis of mouse and human protocadherin gene clusters. *Genome Res* 11:389–404. [CrossRef Medline](#)
- Yokota S, Hirayama T, Hirano K, Kaneko R, Toyoda S, Kawamura Y, Hirabayashi M, Hirabayashi T, Yagi T (2011) Identification of the cluster control region for the protocadherin- $\beta$  genes located beyond the protocadherin- $\gamma$  cluster. *J Biol Chem* 286:31885–31895. [CrossRef Medline](#)
- Young RW (1984) Cell death during differentiation of the retina in the mouse. *J Comp Neurol* 229:362–373. [CrossRef Medline](#)
- Zipursky SL, Sanes JR (2010) Chemoaffinity revisited: dscams, protocadherins, and neural circuit assembly. *Cell* 143:343–353. [CrossRef Medline](#)